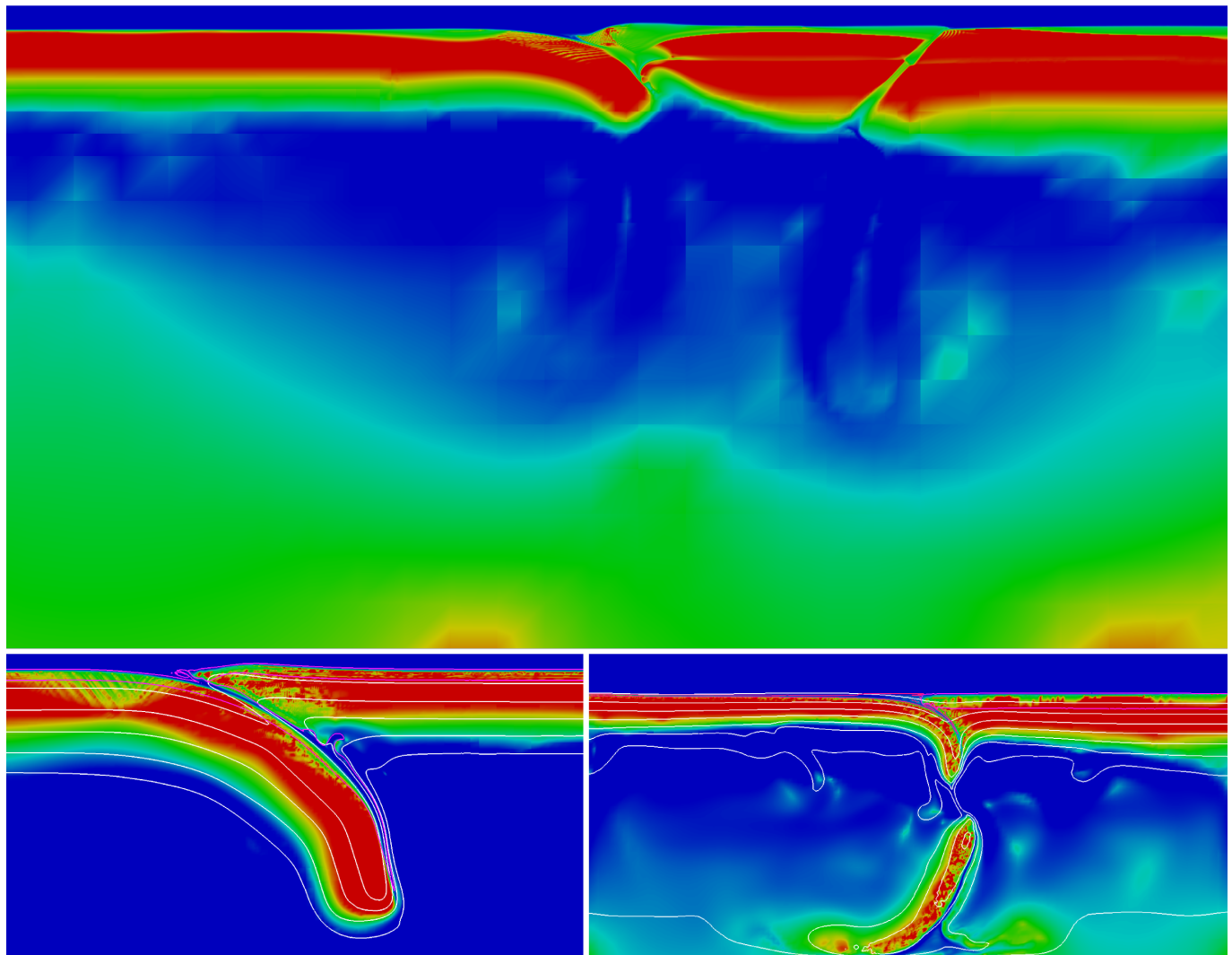


# Thermo-mechanically coupled subduction modelling with ASPECT

Master's thesis by Menno Fraters  
under supervision of Cedric Thieulot, Anne Glerum and Wim Spakman



Department of Earth Sciences  
Utrecht University  
August 2014

# Chapter 1

## Abstract

Subduction is one of the major processes driving the Earth's plate tectonics and is still actively researched in many different fields within the Earth sciences. This report presents a 2D fully thermo-mechanically coupled subduction model with a free surface, using the finite element code ASPECT (short for Advanced Solver for Problem in Earth's ConvecTion). ASPECT is a new finite element code which was originally designed for thermally driven (mantle) convection. It is built on state of the art numerical methods and includes adaptive mesh refinement, linear and non-linear solvers, stabilisation of transport dominated processes and a high scalability on multiple processors. The presented thermo-mechanically coupled subduction model contains four different materials: a crust for the subducting plate, a crust for the overriding plate, a mantle and a sticky air layer. The sticky air layer allows for topography buildup. The extend of the lithosphere into the mantle is mainly defined by the temperature. The initial temperature within our model assumes an adiabatic temperature profile for the mantle, a linear temperature for the lithosphere, and a slab with a linear temperature which has been heated when it descended into the mantle. The viscosity of the materials is defined by visco-plastic rheology using power-law creep and a Mohr-Coulomb criterion. The model contains a free-slip boundary condition at the bottom, an open boundary at the top and an inflow/outflow velocity boundaries at the sides.

The presented model is applied to an investigation of the Western Mediterranean subduction and rollback. During the rollback of the subducting slab beneath Iberia, Corsica and Sardinia were pulled of the northern part of Iberia. To simulate this geological process has proved to be numerically challenging. In this case study the Western Mediterranean setting is investigated. Also an attempt is made to investigate the influence of a weak-zone in the lithosphere.

# Contents

|   |           |
|---|-----------|
| <b>1 Abstract</b>   | <b>1</b>  |
| <b>2 Introduction</b>   | <b>4</b>  |
| 2.1 Modelling plate tectonics . . . . .   | 4         |
| 2.2 Model design . . . . .  | 4         |
| 2.3 Model development for a case study subduction . . . . .                       | 5         |
| <b>3 ASPECT and extensions</b>  | <b>7</b>  |
| 3.1 ASPECT . . . . .  | 7         |
| 3.1.1 Physics of ASPECT . . . . .   | 7         |
| 3.1.1.1 The basic equations . . . . .   | 7         |
| 3.1.1.2 Simplifying the basic equations . . . . .                                 | 8         |
| 3.1.2 The code structure and libraries . . . . .                                  | 8         |
| 3.1.3 Discretization of the domain . . . . .                                      | 9         |
| 3.1.3.1 Elements and basis functions . . . . .                                    | 9         |
| 3.1.3.2 Grid, Adaptive Mesh Refinement and the Initial Refinement Steps . . . . . | 10        |
| 3.1.4 Time discretization . . . . .   | 10        |
| 3.1.5 Solvers . . . . .   | 11        |
| 3.1.5.1 Linear Solvers . . . . .  | 11        |
| 3.1.5.2 Solving coupled and nonlinear systems . . . . .                           | 11        |
| 3.1.6 Advection of materials . . . . .  | 12        |
| 3.1.6.1 Material tracking . . . . .   | 12        |
| 3.1.6.2 Advection errors . . . . .  | 13        |
| 3.2 Non-standard extensions to ASPECT . . . . .                                   | 16        |
| 3.2.1 Rheology . . . . .  | 16        |
| 3.2.2 Averaging scheme . . . . .  | 17        |
| 3.3 New extensions to ASPECT . . . . .  | 18        |
| 3.3.1 General subduction plugin for composition . . . . .                         | 18        |
| 3.3.2 General subduction plugin for temperature . . . . .                         | 19        |
| 3.3.3 Weak zone/refinement plugin and adaptations . . . . .                       | 20        |
| 3.3.4 Converged Relative Residual adaptations . . . . .                           | 22        |
| 3.3.5 Initial fraction adaptations . . . . .                                      | 23        |
| 3.3.6 Maximum timestep adaptations . . . . .                                      | 23        |
| 3.3.7 Line of tracers plugin and adaptations . . . . .                            | 23        |
| 3.3.8 Stokes iterations adaptations . . . . .                                     | 23        |
| 3.3.9 IRS increasing maximum nonlinear iterations adaptations . . . . .           | 24        |
| 3.3.10 Visualisation of normal deviatoric stress plugin . . . . .                 | 24        |
| 3.3.11 Extra output adaptations . . . . .   | 24        |
| <b>4 General subduction modelling</b>   | <b>25</b> |
| 4.1 Introduction . . . . .  | 25        |
| 4.1.1 General setup of the system . . . . .                                       | 25        |
| 4.1.2 Boundary conditions . . . . .   | 25        |

|                     |  |           |
|---------------------|--|-----------|
| 4.2                 | General subduction modelling . . . . .                     | 25        |
| 4.2.1               | Setup . . . . .  | 26        |
| 4.2.2               | General subduction modelling results . . . . .             | 26        |
| 4.3                 | Surface study with passive tracers . . . . .               | 27        |
| 4.4                 | Tolerance Study . . . . .                                  | 29        |
| 4.4.1               | Setup . . . . .  | 29        |
| 4.4.2               | Results . . . . .  | 30        |
| 4.5                 | Timing Study . . . . .                                     | 36        |
| 4.5.1               | Limiting the IRS . . . . .                                 | 36        |
| 4.5.2               | To relax or not to relax . . . . .                         | 37        |
| 4.5.3               | A relative residual study . . . . .                        | 37        |
| 4.6                 | Towards a Western Mediterranean case study . . . . .       | 38        |
| 4.6.1               | Geological setting . . . . .                               | 38        |
| 4.6.2               | Setup . . . . .  | 39        |
| 4.6.3               | Results . . . . .  | 40        |
| <b>5</b>            | <b>Discussion</b>  | <b>45</b> |
| 5.1                 | General discussion . . . . .                               | 45        |
| 5.2                 | Features and evolution of subduction zone models . . . . . | 45        |
| 5.3                 | AMR and plasticity . . . . .                               | 46        |
| 5.4                 | Tracers . . . . .  | 47        |
| 5.5                 | Tolerances and speeding up the model . . . . .             | 47        |
| 5.6                 | Outlook . . . . .  | 48        |
| <b>6</b>            | <b>Conclusions and recommendations</b>                     | <b>51</b> |
| <b>Bibliography</b> |  | <b>52</b> |
| <b>Glossary</b>     |  | <b>57</b> |
| <b>Acronyms</b>     |  | <b>58</b> |

# Chapter 2

## Introduction

### 2.1 Modelling plate tectonics

Since the acceptance of the theory of plate tectonics in the late sixties (Schubert et al., 2001), the field of study and our understanding of the workings of the Earth has expanded dramatically. Subduction is one of the main processes driving plate tectonics and is still subject to a lot of active research (e.g. Strobl et al., 2014; Cai et al., 2014; Song et al., 2014), especially within the geodynamic modelling community (e.g. Cagnioncle et al., 2007; van Keken et al., 2008; OzBench et al., 2008; Schmeling et al., 2008; Herbert et al., 2009; Gerya, 2010; van Hunen and Allen, 2011; Duretz et al., 2012; Jadamec et al., 2013; Baitsch-Ghirardello et al., 2014; Burov et al., 2014; Chertova et al., 2014). The correct modelling of subduction zones remains a challenge due to the amount of processes which might play an important role and the lack of information on the exact conditions and properties of materials within the Earth (Gerya, 2011). This has resulted in a lack of understanding of the relative importance of the different processes associated with subduction and has induced many controversies. These controversies range from the initiation of subduction (e.g. Solomatov, 2004; Gurnis et al., 2004; Hansen, 2007; Crameri and Kaus, 2010; Nikolaeva et al., 2011) to its evolution (e.g. Behounkova and Čížková, 2008; Loiselet et al., 2010; Capitanio et al., 2007) and even its termination (e.g. Baumann et al., 2008; Duretz et al., 2011; Burkett and Billen, 2010; van Hunen and Allen, 2011). The lack of information makes the amount of parameters (parameter space) to investigate, in models which try to incorporate all of the important processes, very large. To be able to systematically investigate the whole parameter space of a certain model, many processes are simplified or ignored. The danger in this approach lies in oversimplification, where the model may not represent a natural subduction zone (Gerya, 2011).

### 2.2 Model design

The subduction model presented and discussed in this thesis is designed to lay in the middle of these two end-members, very complex and overly simple. It contains a complex non-linear rheology, a free surface and several different materials with their own properties, but it does not contain processes like phase changes, strain-weakening, melting and water transport along the subduction wedge.

The model is built with a new code called ASPECT (short for Advanced Solver for Problems in Earth's ConvecTion, Kronbichler et al., 2012). ASPECT is a Finite Element Method (FEM) type of code and is mainly designed for convection problems in the Earths mantle. It is built on the following principles (Bangerth et al., 2014):

1. *Usability and extensibility*

These qualities are expressed in two ways: in the input file and in the modular structure of the code. The input file is a structured file in which the parameters a model uses can be easily changed between models. The modular structure is realised with the use of plugins. Plugins are small parts of code

designed to do one thing only. This can be for example calculating the initial temperature at a certain location. These plugins in combination with the structured input file make it very easy to alter the behaviour of a model by changing parameter values in the input file and/or adding or removing some plugins.

## 2. *Modern numerical methods*

ASPECT has implemented the following modern numerical methods: Adaptive Mesh Refinement (AMR), linear and nonlinear solvers and stabilisation of transport-dominated processes. These methods will be explained in section 3.1.

## 3. *Parallelism*

Because geodynamic models are usually very large and complex, they can not be solved on one processor within a reasonable timescale. It is therefore crucial to distribute the work efficiently among many processors. ASPECT has been designed from the start to be massively parallel. It supports at least up to a thousand processors to work together in an efficient way.

## 4. *Building on others work*

ASPECT is built upon several well documented and tested libraries (collections of code). These libraries are all well supported by an active community of developers. This makes ASPECT on its own a small and focused code with the advantage that it can also automatically benefit from the improvements made in the underlying libraries.

ASPECT is a code that is still under development. This means that subsequent versions may differ a lot in capabilities. For this thesis, the version of 9 December 2013 (revision 2111) was used. Since December 2013, the ASPECT developers have made a lot of improvements and have added functions like phase changes and a true free surface where the surface grid points can deform to the velocity field.

## 2.3 Model development for a case study subduction

The capabilities of the presented modelling framework of plugins and adaptations to ASPECT developed here are illustrated by a potential case study of the Western-Mediterranean subduction and subsequent rollback focused on the region above the North Balearic Transform zone (NBTZ) (see figure 2.1). The lithosphere in this region of the Mediterranean started subducting below Iberia between 85 Ma and 45 Ma. It was initially forced by a very slow convergence of Africa and Europe (Faccenna et al., 2001a,b, 2004; Handy et al., 2010; Carminati et al., 2012; van Hinsbergen et al., 2014). At the onset of rollback at  $\sim 30$  Ma, Sardinia and Corsica were detached from Iberia. This detachment happened along a pre-existing lithospheric fault (Advokaat et al., 2014). The rollback of the subduction zone halted for several millions of years and then continued without Corsica and Sardinia (Faccenna et al., 2001a,b; Spakman and Wortel, 2004; van Hinsbergen et al., 2014). The exact timing and geometry of these events are still under debate. For an overview on the debate of the timing and geometry of subduction and rollback in the Western Mediterranean, the reader is referred to van Hinsbergen et al. (2014).

To realise a detachment of the Sardinia and Corsica block from Iberia, a large lithospheric fault as an initial condition in the model is required, since the initiation of lithospheric scale faults is unlikely to form in stable and homogeneous inner parts of the continental lithosphere (Govers and Wortel, 1995). The role of these lateral heterogeneities in the overriding plate on overriding plate dynamics and subduction dynamics are investigated. Initial modelling towards setting up such a case study will be presented. Time limitation prevented conducting a complete case study.

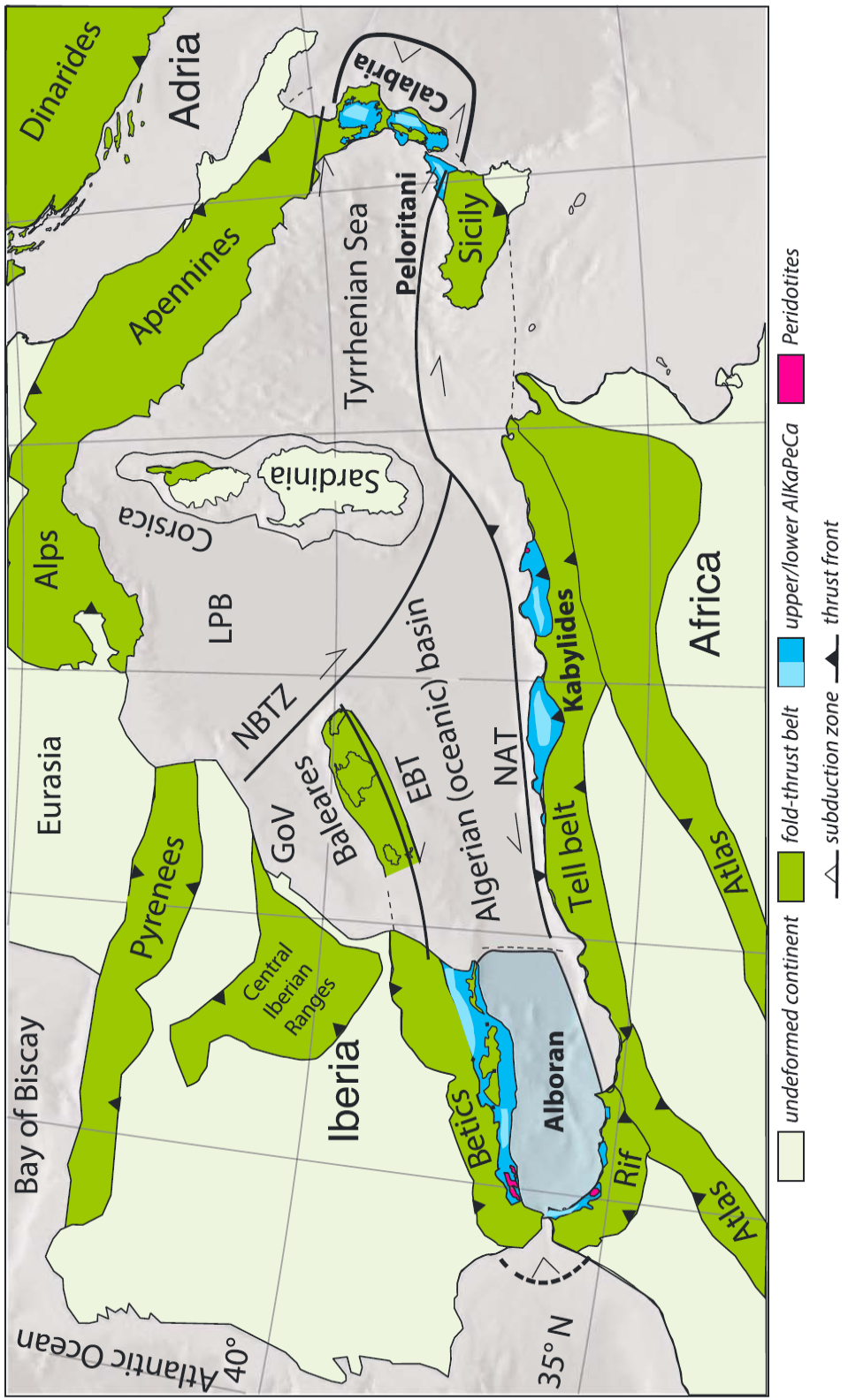


Figure 2.1: Schematic tectonic map of the western Mediterranean region by (van Hinsbergen et al., 2014). EBT = Emile Baudot Transform; LPB = Liguro-Provençal Basin; GoV = Gulf of Valencia; NAT = North African Transform; NBTZ = North Betic Transform Zone.

# Chapter 3

## ASPECT and extensions

The finite element code ASPECT (Kronbichler et al., 2012), the external plugins (Glerum, 2014), the new presented plugins and the presented model all uses certain physics, assumptions and methods. These, as well as the purpose and functions of the plugins, will be explained in this chapter. For a more comprehensive description of the methods used in ASPECT see Kronbichler et al. (2012) and Bangerth et al. (2014). An overview of symbols and physical quantities used in this thesis, together with the units and a short description, is given in table 3.1.

### 3.1 ASPECT

#### 3.1.1 Physics of ASPECT

ASPECT, like other geodynamics codes that solve the Stokes equation, assumes that the solid Earth materials can be treated as a highly viscous fluid. This assumption ensures that the solid Earth can be treated as a fluid in the mathematical description of continuum mechanics. Within this formulation the conservation of momentum, mass and energy have to be considered (Schubert et al., 2001).

##### 3.1.1.1 The basic equations

For the conservation of momentum, mass and energy, ASPECT uses respectively equations (3.1), (3.2) and (3.3). The second and third term on the right hand side (rhs) of Eq. (3.3) represent respectively the shear-heating and the adiabatic heating. Equation (3.4) represents the advection of the compositional fields. Equations (3.1) and (3.2) together form the Stokes equation.

$$-\nabla \cdot \left[ 2\eta \left( \dot{\epsilon}(\mathbf{u}) - \frac{1}{3}(\nabla \cdot \mathbf{u})\mathbf{1} \right) \right] + \nabla p = \rho \mathbf{g} \quad \text{in } \Omega, \quad (3.1)$$
$$\nabla \cdot (\rho \mathbf{u}) = 0 \quad \text{in } \Omega, \quad (3.2)$$

$$\begin{aligned} \rho C_p \left( \frac{\partial T}{\partial t} + \mathbf{u} \cdot \nabla T \right) - \nabla \cdot k \nabla T &= \rho H \\ &\quad + 2\eta \left( \dot{\epsilon}(\mathbf{u}) - \frac{1}{3}(\nabla \cdot \mathbf{u})\mathbf{1} \right) : \left( \dot{\epsilon}(\mathbf{u}) - \frac{1}{3}(\nabla \cdot \mathbf{u})\mathbf{1} \right) \quad (3.3) \\ &\quad + \alpha T (\mathbf{u} \cdot \nabla p) \end{aligned}$$

$$\frac{\partial c_i}{\partial t} + \mathbf{u} \cdot \nabla c_i = 0 \quad \text{in } \Omega, i = 1 \dots C \quad (3.4)$$

### 3.1.1.2 Simplifying the basic equations

As a first order approximation, the lithosphere and mantle can be treated as incompressible fluids. This is commonly done through the Boussinesq approximation (Boussinesq, 1897), the extended Boussinesq approximation or the anelastic approximation. For all the variations on these methods see Ismail-Zadeh and Tackley (2010).

The Boussinesq approximation assumes that the density in all equations except for the rhs of Eq. (3.1) is constant. This rhs term represents small temperature-driven buoyancy (Schubert et al., 2001). The main consequence of this approximation is that Eq. (3.2) can be simplified to Eq. (3.5).

$$\nabla \cdot \mathbf{u} = 0 \quad (3.5)$$

Combining Eq. (3.5) and Eq. (3.3) allows the shear-heating to be dropped from the equation. In the Boussinesq approximation, also the adiabatic term is also dropped. For the consequences of using the Boussinesq approximation, the reader is referred to Hetényi et al. (2011).

The extended Boussinesq approximation brings back the shear-heating term and the adiabatic heating term into the equation. The anelastic approximation assumes that the density is dependent on depth.

The temperature dependent density of the rhs of Eq. (3.1) is usually implemented in the form of the linear Eq. (3.6). In this equation  $\rho_{ref}$  is a reference density at a reference temperature  $T_{ref}$ .

$$\rho = \rho(T) = \rho_{ref}(1 - \alpha(T - T_{ref})) \quad (3.6)$$

In ASPECT it is possible to either use the compressible or incompressible formulations of these equations. In the incompressible case, it is possible to use both the Boussinesq and the extended Boussinesq approximation, in which shear-heating and adiabatic heating can be turned on and off separately. All the models shown in this thesis use the extended Boussinesq approximation, with both adiabatic heating and shear heating.

### 3.1.2 The code structure and libraries

ASPECT is built in a very modular manner. It contains a small core code, which solves the basis equations, serves as a platform for plugins to be attached to and communicates with the libraries on which ASPECT relies that are listed below:

- **DEAL.II** (Bangerth et al., 2007): DEAL.II is a general purpose finite element library. It communicates for ASPECT with other libraries and implements the use of meshes built by p4est, finite elements and discretization.
- **TRILINOS** (Heroux et al., 2005): This library contains code to perform linear algebra calculations in a scalable and parallel way. It provides solvers to ASPECT, which can be used to efficiently solve the equations presented in section 3.1.1 in parallel.
- **p4est** (Burstedde et al., 2011): This library contains code to build distributed adaptive meshes in parallel (more on adaptive meshes in section 3.1.3.2).

The use of libraries in numerical codes has both advantages and disadvantages. Disadvantages are that the installation process can also become more difficult due to the required installation of the libraries. The update process can become more difficult due to compatibility issues between the different versions of the libraries and the code. Advantages are firstly that the code of ASPECT itself remains very compact and understandable, because it only has to focus on the high level implementation of the equations and processes. Secondly, ASPECT can automatically benefit from any improvement in the underlying libraries, with an

additional advantage that these libraries also have much larger and more specialised communities who build and support them.

Plugins in ASPECT are small pieces of code which have a single function and which can be attached or detached from the core of ASPECT easily. An example of such a plugin is a plugin which calculates the initial temperature field within the model. By switching plugins it is very easy to change the behaviour of the model. A major advantage of this structure is that a completely different implementation of calculations or processes within a plugin does not require the other parts of the code to be adapted to those changes.

ASPECT relies on MPI (short for Message Passing Interface) for the distribution of the computation over several processors. ASPECT has been build from the beginning with the parallelism of the code in mind. The domain is divided in small subdomains, which are each processed by a different processor. The implementation has shown to scale well up at least a 1000 processors (Kronbichler et al., 2012).

It is often required to change a lot of parameters between model runs. To prevent constant recompiling of the code, ASPECT reads, every time a model is started, an external input file, in which many runtime parameters can be defined by the user. The parameters in the input file are ordered in subsections, except for the global parameters, which are outside the subsections. It is possible for parameters to be defined within a subsection of a subsection. An example of the structure of an input file can be found in listing 3.1.

Listing 3.1: Example of the structure of a input file.

```

set Dimension = 2
set End time = 2e9
set Output directory = output

subsection Geometry model
    set Model name = box
    subsection Box
        set X extent = 1600000.0
        set Y extent = 760000.0
    end
end

subsection Mesh refinement
    set Initial global refinement = 4
    set Initial adaptive refinement = 1
end

subsection Postprocess
    set List of postprocessors = all
end

```

### 3.1.3 Discretization of the domain

#### 3.1.3.1 Elements and basis functions

To solve a model problem numerically with the FEM, the domain has to be broken up (discretized) along a defined grid. Basis functions have then to be defined for the independent variables (the independent directions of the velocity -in 2D two and in 3D three- the pressure and the temperature). Finite element codes often use linear basis functions for the velocity and piecewise constant basis functions for the pressure ( $Q_1 P_0$ ) (Thieulot, subm; Kronbichler et al., 2012). Because this approach violates a stability condition called the Ladyzhenskaya, Babuska and Brezzi (LBB) condition (Donea and Huerta, 2003), ASPECT uses instead so-called  $Q_2 Q_1$  elements which do not violate this condition (Kronbichler et al., 2012).  $Q_2 Q_1$  elements consist of quadratic basis functions for the velocity and linear basis functions for the pressure. Although this approach is more accurate, the use of  $Q_2 Q_1$  elements compared to  $Q_1 P_0$  will also increase the computational effort, as the number of unknowns, also called Degrees of Freedom (DoF), is much larger

per element in  $Q_2 Q_1$  elements. This is due to the fact that a quadratic basis function contains 9 points per element. Thus, for the 2D velocity alone, there are 18 unknowns per element, while for a linear basis function there would be only 9. In 3D this difference becomes even larger. ASPECT also uses  $Q_2$  elements for the temperature.

### 3.1.3.2 Grid, Adaptive Mesh Refinement and the Initial Refinement Steps

The grid, on which the model is defined, is initially always a regular grid, where all the cells have the same height and the same width (and in 3D also the same depth). Although it is perfectly possible to use a very fine regular grid for realistic simulations, it is also possible to use a method called Adaptive Mesh Refinement (AMR) in ASPECT. AMR allows the grid to be refined and coarsened locally during the calculations. This method can be a hundred times faster in 2D and up to a thousand times faster in 3D than using a regular grid with the same highest resolution (Kronbichler et al., 2012).

The AMR in ASPECT works in four stages. The first stage is the computation of the error field. The values of the error field can be based on several refinement and/or coarsening criteria. This can be criteria like the temperature gradient or the change from one material (called composition in ASPECT) to an other material. The second step is setting refinement and coarsening flags for the cells based on the constructed error field. The cells which contain the highest fraction of the error field are assigned a refinement flag. The cells which contain the lowest fraction of the error field are assigned a coarsening flag. The third stage is a check in which refinement flags for cells which are already at the maximum refinement are removed. The fourth stage is the actual refinement and coarsening based on the assigned flags. The precise fraction at which a coarsening or refinement flag should be assigned is defined by the user.

The AMR method can also be applied to build the initial grid. The initial grid is built through an iterative process shown in Fig. 3.1. The steps it goes through are called the Initial Refinement Steps (IRS). In the first step a regular grid is build, solved and the error is determined (IRS 1 in Fig. 3.1). Then the grid is refined and coarsened based on the error field (IRS 2 and 3 in Fig. 3.1). This process also continues at a user defined interval during timesteps (see Timestep 1 in Fig. 3.1).

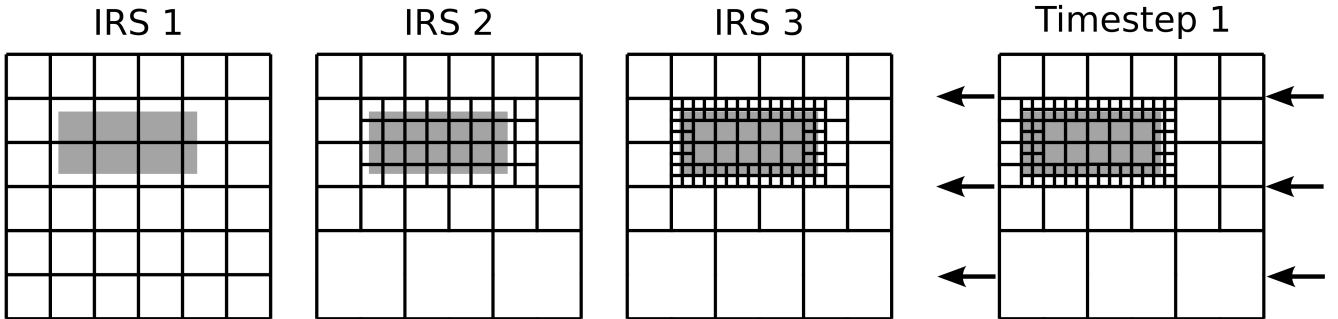


Figure 3.1: Concept figure of the AMR method. An example with two materials, a white and grey material, where the interface between these materials defines the error field. During timestep 1 the materials are advected to the left and the grid has automatically been adapted to the new location of the interface.

### 3.1.4 Time discretization

When models are required to evolve in time, the size of the chosen timestep is very important. If the timesteps are too large, the solution may become completely different compared to a smaller timestep and the solver may not be able to find a good solution. If the timesteps are too small, a lot of computational time will be wasted. A solution to this problem is the use of the Courant-Friedrich-Lowy (CFL) condition (Anderson, 1995). ASPECT makes use of the formulation in Eq. (3.7). The CFL condition must be satisfied

for every cell K in the domain.

$$\frac{\delta t \|\mathbf{u}\|_{\infty, K}}{h_K} \leq C \quad (3.7)$$

In more descriptive terms this CFL condition means that the timestep is chosen in such a way that a point in a cell which is advected, does not move further than C times the diameter of the cell. In normal systems C is chosen between 0 and 1, although in ASPECT values higher than one are stable (Kronbichler et al., 2012). In the models shown in this thesis, C was always set to 0.5.

### 3.1.5 Solvers

#### 3.1.5.1 Linear Solvers

The discretized basis equations can be written into a system of equations. This takes the form of Eq. (3.8), where  $\mathbf{A}$  is a  $n \times n$  matrix, and  $\mathbf{x}$  and  $\mathbf{b}$  are vectors of length n, where n is the number of unknowns in the system. Vector  $\mathbf{b}$  is called the rhs vector and contains the boundary conditions and buoyancy forces. Vector  $\mathbf{x}$  contains the unknowns of the system to be solved, such as velocity, pressure and/or temperature.

$$\mathbf{A} \mathbf{x} = \mathbf{b} \quad (3.8)$$

There are traditionally two main types of solvers to solve this kind of systems of equations: a direct type of solver and an iterative type of solver. The main practical difference between the two methods is that a direct solver gives directly an exact solution to the problem within the calculation precision of the computer. The limitation of this method is that it requires much memory for its calculation. This becomes a problem when the number of unknowns in a system becomes very large, because they then require a lot of computer memory. When simulating realistic problems, this can become a real problem. An iterative solver, unlike a direct solver, does not immediately provide an exact solution to the model problem on its first iteration. Instead it uses the previous solution of vector  $\mathbf{x}$  as a starting condition to solve the system of equations again. It can be proved that under certain conditions, this iterative process, called the inner iterations, will converge to the exact solution (Meister, 1999). The advantage of this method is that much less memory is required, especially in 3D.

To determine if the iterations of an iterative solver can be stopped, it must be determined whether the solution to the model problem is good enough. For this ASPECT uses the linear residual vector  $\mathbf{r}$  of the system defined in Eq. (3.9). When the  $L_2$  norm of vector  $\mathbf{r}$  is smaller than a user defined tolerance, the system is seen as solved. This process is illustrated in the red part of Fig. 3.2.

$$\mathbf{r} = \mathbf{Ax} - \mathbf{b} \quad (3.9)$$

#### 3.1.5.2 Solving coupled and nonlinear systems

With solvers it is possible to acquire a separate solution for both the energy equation Eq. (3.3), which solves for the temperature, and the Stokes equation Eqs. (3.1) and (3.2), which solves for velocity and pressure. Through the basis equations (section 3.1.1), it can be seen that the formulation for the momentum equation, Eq. (3.1), depends on temperature, as explained in section 3.1.1.2. The energy equation, Eq. (3.3), is dependent on the velocity and pressure. These are therefore called coupled equations.

Within the Stokes system, specifically the part of the conservation of momentum, a similar type of dependency problem can occur. This has to do with the fact that viscosity is dependent on stress or strain-rate, which is strongly dependent on the velocity. Although this is not always accounted for in so called linear rheologies, nonlinear rheologies (see section 3.2) do take this into account.

Both the nonlinearity of the coupled Stokes and temperature equations and the nonlinearity of the viscosity need to be iterated out. Since advection is much more important than diffusion in geodynamics models, it can be assumed that the nonlinearities due to the coupling of the temperature and stokes systems will be iterated out over several timesteps, and recalculation of the temperature field is not necessary. The nonlinearities induced by the nonlinear rheology are too strong, and need to be iterated out within a timestep. This scheme is called 'iterated stokes' scheme in ASPECT, and these iterations are called the outer iterations or nonlinear iterations. By default in ASPECT the outer iterations have a stopping criterion based on the  $L_2$  norm of the residual. The residual of the system with its initial zero values is compared to the current residual. This is called the relative residual. When the system has its zero initial values, i.e. all elements in vector  $\mathbf{x}$  in Eq. (3.8) are zero, the error  $\mathbf{r}$  is equal to the solution. If the residual is reduced several order of magnitude, it is likely that the error has also fallen several orders of magnitude (Ismail-Zadeh and Tackley, 2010). When the relative residual is smaller than a user defined value, the nonlinear iterations are stopped.

The iterated Stokes scheme is a scheme which uses Picard type iterations. A schematic overview of this process can be seen in Fig. 3.2. When the inner iterations have converged, first the strain-rate is recomputed. Then, based on the strain-rate, the viscosity is recomputed. If the relative residual ( $\frac{\|R_n\|_2}{\|R_0\|_2}$ ) is not smaller than a user defined value, matrix  $\mathbf{A}$  is updated. This is important because  $\mathbf{A}$  in Eq. (3.8) is dependent on strain-rate and viscosity. With this new  $\mathbf{A}$ , the system is solved again. When the nonlinear iterations have converged, the velocity field is used for advection of the material and some post-processing (e.g. calculating several statistics, advecting passive tracers, making files for visualisation of the data).

### 3.1.6 Advection of materials

#### 3.1.6.1 Material tracking

It is crucial in subduction modelling to be able to track materials. There are several methods available to track one or several materials through a model. The most used method within the geodynamical community is called the marker-in-cell method (e.g. I2ELVIS (Gerya and Yuen, 2003a, 2007), FANTOM (Thieulot, 2011), ELEFANT (Thieulot, subm), UNDERWORLD (Moresi et al., 2003, 2007), CitcomS (Zhong et al., 2000; Tan et al., 2006; McNamara and Zhong, 2004)). A marker, also called a tracer or Lagrangian particle, is a 'physical' particle in the model (see Fig. 3.3 A). This particle can store information about its environment like temperature and pressure and/or can contain parameters like material properties which are used in calculations. These particles are then advected along with the flow.

Note that there are two types of markers: passive and active markers. Passive markers only store environment information as they are advected. The simplest version of passive markers only stores their current location, which can be useful for, for example, tracking a surface. Active markers at least contain some parameters like material properties which are actually used in the solving of the equations.

Another approach to track materials is called the levelsets method (Zlotnik et al., 2008; Braun et al., 2008; Hillebrand et al., subm). Instead of physical points, this method tracks a surface with the value zero (see Fig. 3.3 B). A smooth function (levelset function) is defined through this surface which is on the one side positive and the other side negative. The levelset function represents the distance from the surface. The difference in sign is used to identify the different materials.

ASPECT uses a method numerically similar to the levelset method. Instead of a surface, it tracks one or several fields called phase fields or compositional fields (Lenardic and Kaula, 1993; van Keken et al., 1997; Kronbichler et al., 2012). A field has a value of one inside of a specific material or composition and zero outside (see Fig. 3.3 C). Because of numerical diffusion, all the fields will have values between one and zero near the material interfaces. Furthermore, through advection errors, the fields can locally obtain values higher than one and lower than zero in some cases.

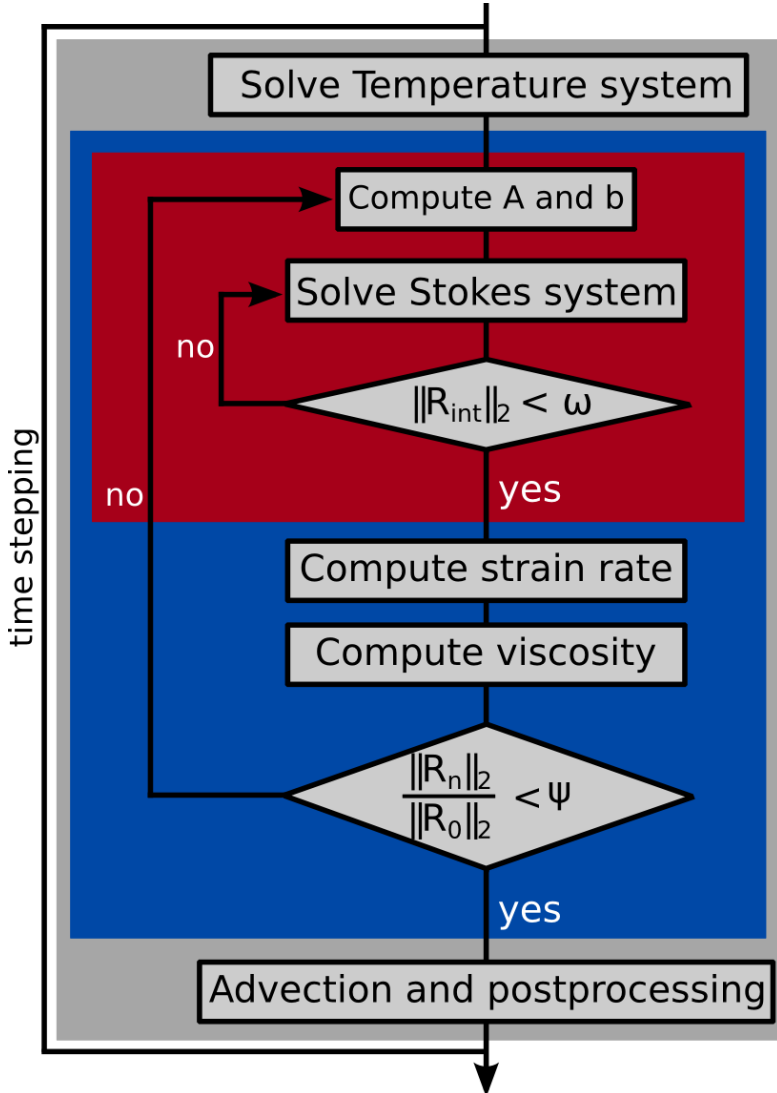


Figure 3.2: A schematic overview of the process of solving the systems of equations for each timestep. The grey part indicates a timestep, the blue part shows the nonlinear iteration part of the Stokes system, and the red part shows the iterative linear solver for the Stokes system. The solving of the temperature system is similar to what is shown in the red part of the Stokes system.

### 3.1.6.2 Advection errors

Advection of materials in numerical models is not trivial as material interfaces on the length scales of geodynamical modelling are discontinuous interfaces. The advection of a steep gradient or even a discontinuous interface is numerically very challenging and often introduces numerical errors into the solution. If not managed well, these errors can quickly grow larger than the solution itself (Lenardic and Kaula, 1993). There are two types of errors associated with the advection of a discontinuous surface (see Fig. 3.4): diffusion errors and dispersion errors. For more information on the nature of these errors, the reader is referred to Lenardic and Kaula (1993). Figure 3.4 shows an example of an undershoot at the location of the dispersion error.

To keep the errors from growing to the same order of magnitude of or larger than the solution, stabilisation is required. This is commonly done by adding numerical diffusion in cells where the Péclet number (as defined in Eq. (3.10), where  $K$  is the cell) is large. The Péclet number is a number which indicates the balance between the advective and the diffusion transport rate. A large Péclet number therefore indicates that there is much advection. Because the risk for unstable behaviour only occurs around a steep gradient, ASPECT has adopted a method from Guermond et al. (2011). This method only adds numerical diffusion

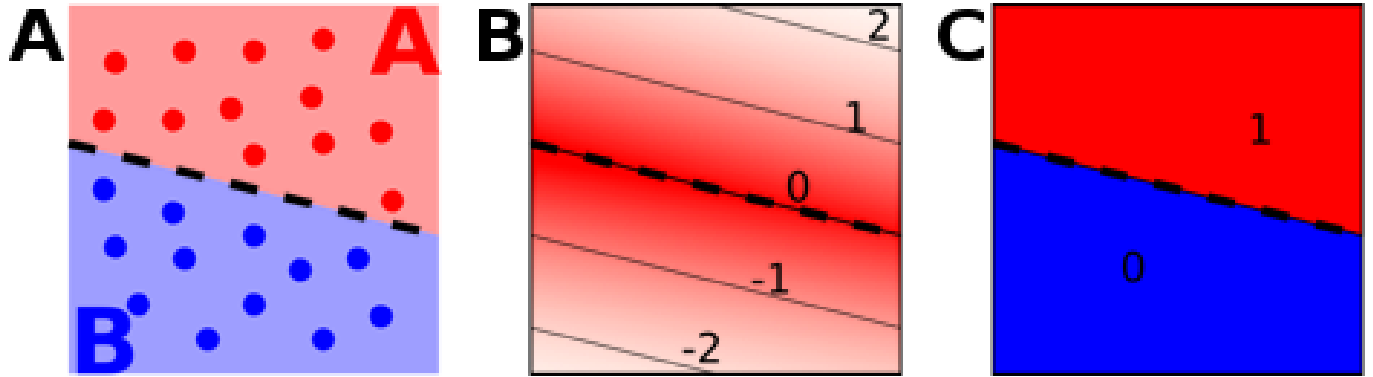


Figure 3.3: Three methods for the definition of materials. Figure A shows tracers, figure B shows a levelset and figure C shows fields. Figure by Bram Hillebrand.

to cells where the local Péclet number is large and the solution is non-smooth (Kronbichler et al., 2012).

$$Pe_K = \frac{h_K |u|_K}{\kappa} \quad (3.10)$$

### ADVECTION OF A STEP FUNCTION

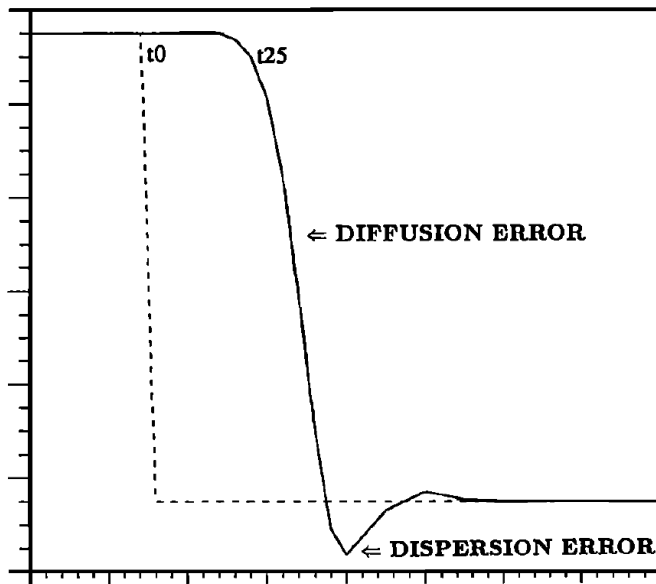


Figure 3.4: Numerical advection of a step function over several timesteps from Lenardic and Kaula (1993).  $t_0$  is the initial step function and  $t_{25}$  the final advected step function. The two common numerical error types (diffusion and dispersion) are shown here.

| <b>symbol</b>          | <b>meaning and dimension</b>                                    |
|------------------------|---|
| $A, A_{df}, A_{ds}$    | Prefactor (diffusion and dislocation) ( $Pa^{-n}s^{-1}$ )       |
| $c_i$                  | Compositional field   |
| $C$                    | Cohesion ( $Pa$ )   |
| $C_P$                  | Specific heat capacity ( $Jkg^{-1}K^{-1}$ )                     |
| $g$                    | Gravity ( $ms^{-2}$ )   |
| $h_k$                  | Diameter of the cell ( $m$ )                                    |
| $H$                    | Internal heat production ( $Wm^{-3}$ )                          |
| $k$                    | Thermal conductivity ( $Wm^{-1}K^{-1}$ )                        |
| $l$                    | Thickness of slab ( $m$ )                                       |
| $n$                    | Powerlaw creep exponent   |
| $p$                    | Pressure ( $Pa$ )   |
| $Q, Q_{df}, Q_{ds}$    | Activation energy (diffusion and dislocation) ( $Jmol^{-1}$ )   |
| $R$                    | Gas constant ( $Jkg^{-1}mol^{-1}$ )                             |
| $T$                    | Temperature ( $K$ )   |
| $T_{pot}$              | Potential temperature at the surface ( $K$ )                    |
| $\mathbf{u}$           | Velocity vector ( $ms^{-1}$ )                                   |
| $v$                    | Velocity ( $ms^{-1}$ )  |
| $V, V_{df}, V_{ds}$    | Activation volume (diffusion and dislocation) ( $m^3mol^{-1}$ ) |
| $\alpha$               | Thermal expansion coefficient ( $K^{-1}$ )                      |
| $\delta t$             | Timestep ( $s$ )  |
| $\dot{\epsilon}$       | Strain rate ( $s^{-1}$ )  |
| $\dot{\epsilon}$       | Strain rate tensor ( $s^{-1}$ )                                 |
| $\dot{\epsilon}'_{II}$ | Second invariant of the strain rate tensor ( $s^{-1}$ )         |
| $\eta$                 | Dynamic viscosity ( $Pas$ )                                     |
| $\theta$               | Dip angle ( $^\circ$ )  |
| $\kappa$               | Thermal diffusivity ( $m^2s^{-1}$ )                             |
| $\lambda$              | Volume (Second or bulk) viscosity ( $Pas$ )                     |
| $\nu$                  | Constant  |
| $\rho$                 | Mass density ( $kgm^{-3}$ )                                     |
| $\sigma$               | Stress tensor ( $Pa$ )  |
| $\sigma'$              | Deviatoric stress tensor ( $Pa$ )                               |
| $\tau$                 | Maximum nonlinear iterations                                    |
| $\phi$                 | Angle of internal friction ( $^\circ$ )                         |
| $\omega$               | Stokes tolerance  |
| $\psi$                 | Nonlinear tolerance   |

Table 3.1: Nomenclature

## 3.2 Non-standard extensions to ASPECT

The models presented in this thesis make use of a non-standard extension from Glerum (2014) to compute the viscosity at every location in the model. This extension is based on a viscoplastic rheology, of which the parameters can be determined per defined composition.

### 3.2.1 Rheology

ASPECT assumes that the Earth materials can be treated as highly viscous fluids, as explained in Section 3.1.1. It is therefore important to define realistic flow laws, i.e. rheological laws, for the materials. There are three main rheological groups of deformations which are often used in the field of geodynamics:

1. **Viscous deformations:** Viscous deformation represents mechanisms which deform the material permanently, without a yielding criterion. There are two deformation mechanisms commonly associated with a viscous rheology, also called powerlaw creep mechanisms:
  - **Dislocation creep** (see the dark grey area in Fig. 3.5): Deformation through this mechanism is caused by deformation of the crystals in the material. This process can be activated at low stresses (Schubert et al., 2001), and is very stress dependent. It is not dependent on grain-size.
  - **Diffusion creep** (see the light grey area in Fig. 3.5): Deformation through this mechanism works through the movement of vacancies, i.e. the filling of vacancies which causes the opening of new vacancies, through the material. This process is linearly dependent on stress and strongly dependent on grain-size (Kameyama et al., 1999; Karato, 2008).
2. **Plastic deformations:** Plastic deformation, like viscous deformation, deforms the material permanently. The difference is that this mechanism becomes active after it has surpassed a certain yielding criterion. This mechanism is mainly active at very shallow depths and limits the shear stress (Garel et al., 2014). There are two mechanisms often used to model this type of deformation:
  - **Mohr-Coulomb criterion:** The yielding with the Mohr-Coulomb criterion is based on the angle of internal friction and the cohesion, and simulates the brittle behaviour of rock.
  - **Peierls creep**(see the white area in Fig. 3.5): Peierls creep is physically similar to dislocation creep. It occurs due to the glide motion of dislocations without recovery (Garel et al., 2014). This process is, compared to dislocation creep, less sensitive to temperature and more sensitive to stress (Garel et al., 2014; Karato, 2008).
3. **Elastic deformations:** This represents the elastic behaviour of solid materials, where the deformation of the material can be recovered. This is usually seen as a short timescale effect (Schubert et al., 2001). ASPECT is currently not capable of modelling elastic deformation.

The external plugin by Glerum (2014) implements a viscoplastic rheology. The viscous part models diffusion creep (formula 3.11) and dislocation creep (formula 3.12). The plastic part is modelled by a Mohr-Coulomb criterion (formula 3.14). Because the implementation of Peierls creep will be similar to diffusion creep and dislocation creep, it is considered to be trivial to implement it, but it has not been done yet. Equations (3.11), (3.12) and (3.14) are combined to calculate the effective viscosity in a viscoplastic case (equation 3.13). In Eqs. (3.11) to (3.14)  $df$  stands for diffusion creep,  $ds$  stands for dislocation creep,  $c$  indicates that this value is determined by the averaging scheme which is used (see section 3.2.2).

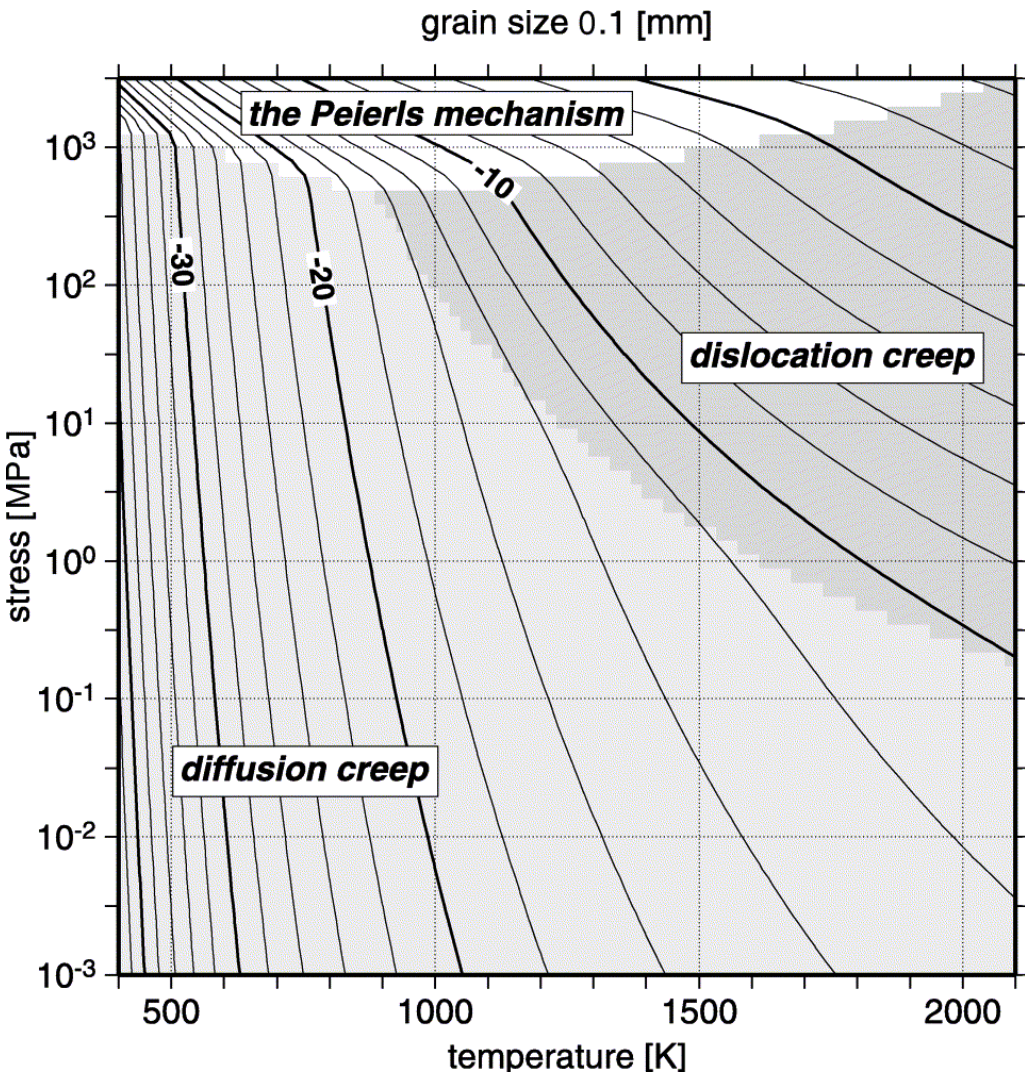


Figure 3.5: Deformation mechanism map calculated for grain size  $a=0.1$  mm. The lightly shaded area indicates that deformation mainly occurs by diffusion creep. The densely shaded area indicates that deformation mainly occurs by power-law creep. The white region indicates that deformation mainly occurs by the Peierls mechanism. The solid curves are lines of constant strain rate. The numbers attached to each contour indicate the logarithm of the strain rate in the unit of  $s^{-1}$ . (From Kameyama et al., 1999)

$$\eta_{diff} = \frac{1}{2} \frac{1}{A_{df\_c}} * \exp\left(\frac{Q_{df\_c} + V_{df\_c}P}{RT}\right) \quad (3.11)$$

$$\eta_{disl} = \frac{1}{2} \nu_{ds\_c} A_{ds\_c}^{\frac{-1}{n\_c}} * \max(\dot{\epsilon}'_{II}, \epsilon_{min})^{\frac{1-n_c}{n_c}} * \exp\left(\frac{Q_{ds\_c} + V_{ds\_c}P}{n_c RT}\right) \quad (3.12)$$

$$\eta_{eff} = \min\left(\frac{1}{\frac{1}{\eta_{diff}} + \frac{1}{\eta_{disl}}}, \eta_{plastic}\right) \quad (3.13)$$

$$\eta_{plastic} = \frac{P \sin(\phi_c) + C_c \cos(\phi_c)}{2.0 * \max(\dot{\epsilon}'_{II}, \epsilon_{min})} \quad (3.14)$$

### 3.2.2 Averaging scheme

The use of Eqs. (3.11) to (3.14) is trivial when an element contains only one composition, but this is not always true. In these cases an averaging scheme has to be used. In this extension, two averaging schemes have been implemented:

- **Max rule:** This rule takes the values of the composition which has the highest value at that point. See equation 3.15, where in this case  $n$  is the amount of viscosity values and  $a$  are the viscosity values.
- **Weighted harmonic averaging:** This is a more general case of the often used harmonic averaging. The formulation for the weighted harmonic averaging is shown in Eq. (3.16), where in this case  $n$  is the amount of viscosity values,  $a$  are the viscosity values and  $w$  are the compositional values. This averaging scheme tends to soften large outliers in its data set and is in all cases equal or lower than a geometric or arithmetic averaging scheme. The in geodynamics often used harmonic averaging, Eq. (3.17), is a special case where all the weights are one.

$$M_\infty = \max(a_1, a_2, \dots, a_n) \quad (3.15)$$

$$M_{-1} = \frac{w_1 + w_2 + \dots + w_n}{\frac{w_1}{a_1} + \frac{w_2}{a_2} + \dots + \frac{w_n}{a_n}} \quad (3.16)$$

$$M_{-1} = \frac{n}{\frac{1}{a_1} + \frac{1}{a_2} + \dots + \frac{1}{a_n}} \quad (3.17)$$

For a more general formulation of non-weighted average schemes see Thieulot (subm). Although some models have been tested with the max-rule, the harmonic averaging has been used for all the models presented in this thesis.

Equations (3.15) and (3.17) give in practice very high and low values for the viscosity. This can become a problem because the solver can not handle too large differences in the viscosity. That is why the resulting viscosity is cut off at a user defined minimum and maximum value.

### 3.3 New extensions to ASPECT

In this section, the plugin and adaptations written specifically to model a termomechanical subduction are described.

#### 3.3.1 General subduction plugin for composition

The general subduction plugin for composition implements a basic subduction distribution for the composition field, as can be seen in Fig. 3.6. It uses the first four compositions defined in the plugin in Section 3.2 and uses them for the mantle composition, the subducting crust composition, the overriding crust composition and the sticky air composition respectively.

Sticky air, or sticky water, is a term used for a low viscosity layer on top of a model. The purpose of this layer is to generate topography on top of the model, without having to deform the grid (Zaleski and Julien, 1992; Gerya and Yuen, 2003b; Schmeling et al., 2008; Quinquis et al., 2011; Crameri et al., 2012). Because the solving of areas with very high viscosity contrasts is very hard, high viscosities for the air/water layer have to be chosen. The viscosity chosen for this layer is therefore much larger than what it would be in reality for air or water, usually in the order of  $10^{18}$  to  $10^{20}$  Pas. It is important to have about five orders of magnitude difference between the sticky air layer and the surface to be deformed (Crameri et al., 2012). The sticky air layer must also be thick enough. This thickness can be greatly reduced if the top boundary velocity condition is open (Hillebrand et al., subm).

The plugin allows for much customisation of the setup in the input file. The user can define the location of the subduction zone, angle and length of the subducting part of the crust, the thickness of the crust layers and the sticky air layer and the radius of the smoothing circle (Fig. 3.6).

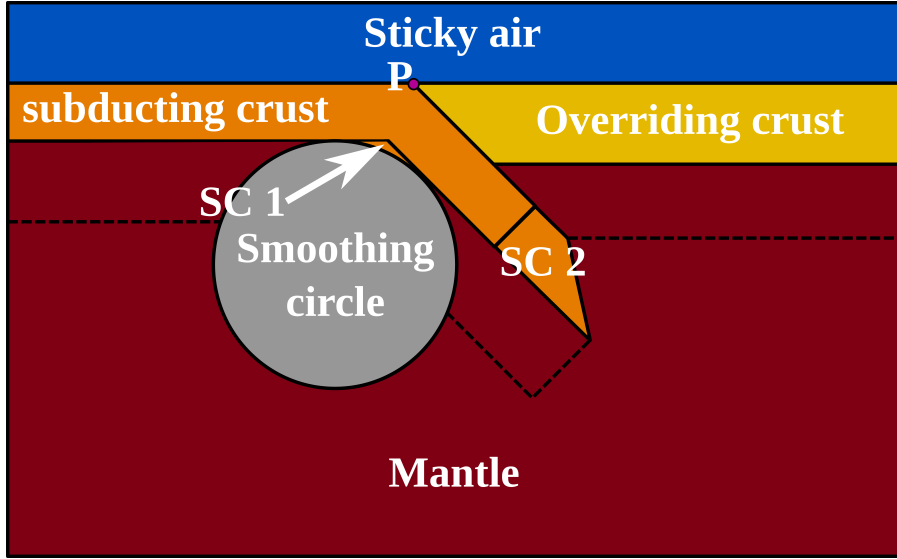


Figure 3.6: A schematic figure for the distribution of compositions created by the general subduction plugin for composition. It contains a sticky air layer (blue), a mantle part (dark red), a subducting plate crust (orange) and a overriding plate crust (yellow). The dashed lines show the extend of the lithosphere. The circle in grey illustrates how the transition from crust on the surface to subducting crust is smoothed by creating a bit of extra subducting crust (SC 1). SC 2 shows what happens if the slab is defined by the user so long that it come out under the overriding lithosphere. It is thinned by a linear function from the point it comes out under the overriding lithosphere, to where the crust is supposed to stop. The purple point P indicates a rotation point, where the slab is rotated from.

### 3.3.2 General subduction plugin for temperature

The general subduction plugin for temperature implements an initial temperature distribution for a basic subduction setting. The sticky air layer is assigned the temperature of the top boundary. The initial mantle temperature is modelled as an adiabatic temperature according to Eq. (3.18). The temperature of the lithosphere in the parts which are not subducting is defined by a linear temperature gradient from the surface temperature to the mantle temperature at the bottom of the lithosphere. The subducting part of the lithosphere is modelled by the McKenzie (1970) temperature formula, Eqs. (3.19) to (3.23). These equations calculate a non-dimensionalized temperature for a non-dimensional warming half-space, which had an initial linear temperature distribution. It simulates old lithosphere entering the mantle and warming up. The thickness of the lithospheric layers, the dip of the subducting slab and the velocity with which the lithospheric slab was subducting can all be set by the user.

$$T = T_{pot} + \frac{T_{pot}\alpha g}{C_p} (depth_{model} - depth_{current}) \quad (3.18)$$

$$T(x', z') = \exp\left[\frac{x' \sin\phi - z' \cos\phi}{h'}\right] \times [T_{pot} + 2(T_{pot} - 273) \sum_{n=1}^{\infty} \frac{(-1)^n}{n\pi} \exp(R - \sqrt{R^2 + n^2\pi^2}) x' \sin(n\pi z')] \quad (3.19)$$

$$R = \frac{\rho C_P v l}{2\kappa} \quad (3.20)$$

$$h' = \frac{C_P}{\alpha g l} \quad (3.21)$$

$$lx' = x \quad (3.22)$$

$$lz' = z \quad (3.23)$$

### 3.3.3 Weak zone/refinement plugin and adaptations

To allow for weak zones, i.e. localised areas where the material is weaker, and for localised refinement, several plugins had to be created and adaptations to the code and other plugins had to be made. Although the weak zone/refinement plugin is built to create weak zones and/or locally refined areas, it can overwrite almost any field in ASPECT. The overwriting of the fields is done just before the plugin responsible for that field sends the value back to the core of ASPECT. The plugin and adaptions are currently only available in 2D. The area to be overwritten is definition through the following process:

1. Define at what point of a rectangle (see Fig. 3.7 A) the area should rotate from. Use the number for that point as indicated in Fig. 3.7. This is called the **rotation-point**.
2. Define where this rotation-point should be within the domain. This is called the begin-point.
3. Define the length and thickness of the rectangle area.
4. Define what kind of shape the area should have. This shape is defined within the previously defined area. The default is a rectangle (Fig. 3.7 B1), but other shapes can be cut out of the rectangle, such as an ellipsoid (Fig. 3.7 B2) and a triangle (Fig. 3.7 B3). The triangle can point up ,down, to the right and to the left.
5. Define the angle the rectangle is to be rotated over from the rotation point (Fig. 3.7 C).
6. Define an upper and lower limit (relative to the whole domain) where the area to overwrite must fall within.

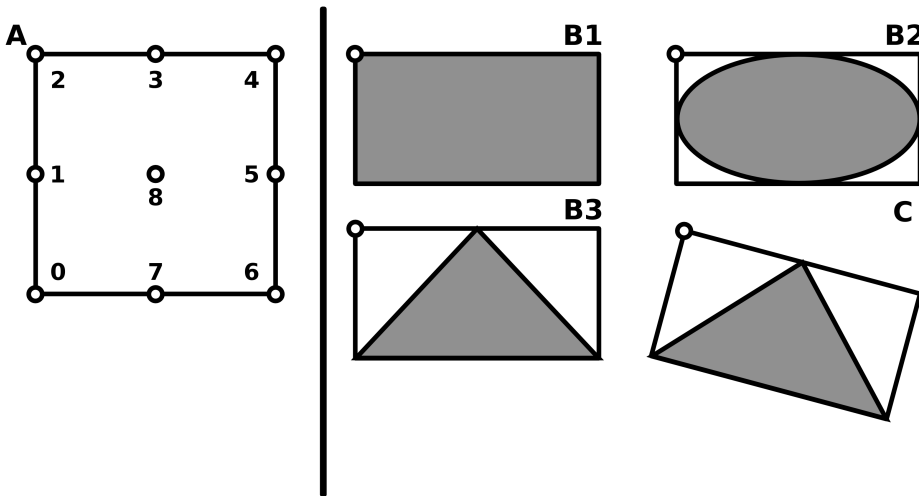


Figure 3.7: A schematic figure illustrating parts of the process of setting up a weak zone. Figure A shows the possible rotation points which can be used. Figure B1 to B3 show different kind of features which can be cut out of the rectangle, where the grey area is the area in which a field needs to be changed. Figure C shows the use of the defined rotation point to rotate the grey area.

After the area in which the field has to be changed is defined, the user can define which field(s) needs to be changed, and in what way. The following four fields can be changed and are discussed below: viscosity, refinement error, initial temperature and composition:

- **Viscosity:** The user can define how much the material in this area should be weakened. This can be done with Eq. (3.24), where  $W$  is the user defined weakening and  $M$  is a multiplier.

$$\eta = \frac{\eta}{W * M} \quad (3.24)$$

To prevent large viscosity jumps at the edges of the defined weak zone, the multiplier  $M$  can be used to soften these boundaries. For this purpose, two different methods have been implemented. The first

method (see Fig. 3.8 with the X:Y 0.1:0.1 to 1000:1000) uses exponential function Eqs. (3.25) to (3.27), where  $OF_x$  and  $OF_y$  are respectively the exponent, or order function, for the x-axis and y-axis and  $pmin_x$  and  $pmin_y$  are the most 'left'/lowest x value side and the bottom side of the rectangle.

$$M = \min(M\_x, M\_y) \quad (3.25)$$

$$M\_x = (1 - \text{abs}\left(\frac{x_{\text{rot}} - pmin_y - 0.5 * \text{thickness}}{0.5 * \text{thickness}}\right)^{OF_x}) * W \quad (3.26)$$

$$M\_y = (1 - \text{abs}\left(\frac{y_{\text{rot}} - pmin_x - 0.5 * \text{thickness}}{0.5 * \text{thickness}}\right)^{OF_y}) * W \quad (3.27)$$

The second method (see Fig. 3.8 with  $10^{(ax+b)}$ ) is based on Eqs. (3.28) to (3.31), and creates a smooth transition all around the weak zone.

$$M = 10^{ax+b} \quad (3.28)$$

$$a = \log_{10}(W) \quad (3.29)$$

$$x = \left(\frac{x_{\text{rot}} - pmin_x}{0.5 * \text{length}}\right)^2 + \left(\frac{y_{\text{rotated}} - pmin_y}{0.5 * \text{thickness}}\right)^2 \quad (3.30)$$

$$b = \log_{10}\left(\frac{\eta}{W}\right) \quad (3.31)$$

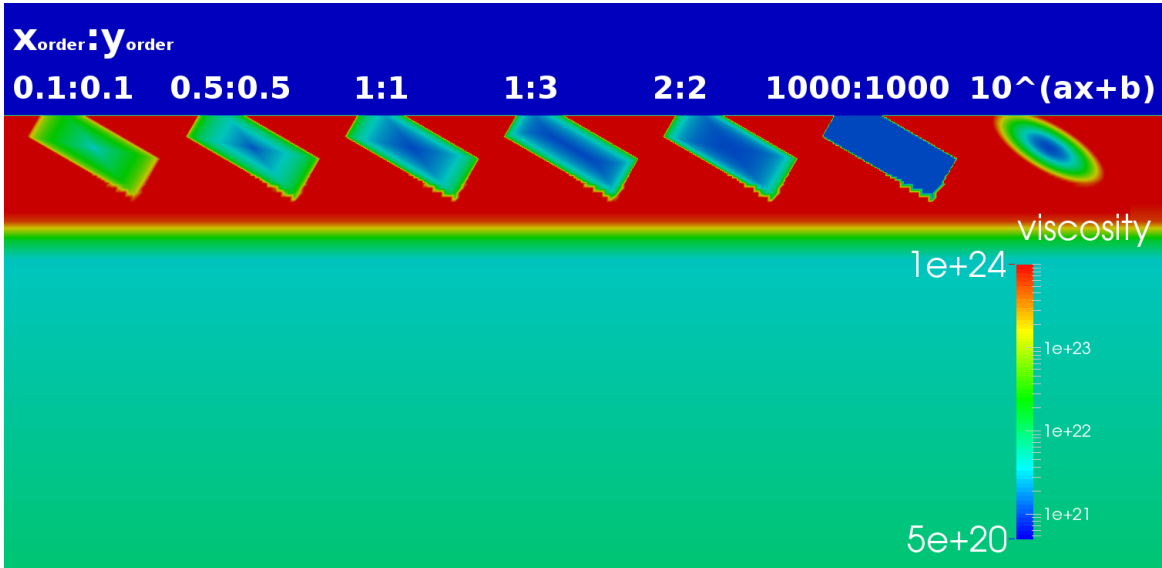


Figure 3.8: An illustration of the use of weak zones to change the viscosity locally and the difference between the order functions. Note that the scale has been adapted, from a minimum of  $1e19$  to a minimum of  $5e20$ , to show the effect more clearly.

- **Refinement error:** This can be used to add to the error, which is used to refine and coarsen the grid of the model. The error value is determined per element, and it is therefore necessary to calculate if the area of the element overlaps with the area which gains in error value. This is not trivial, and therefore three steps are used:

1. Look if a vertex of the cell is in the refinement area. If this is true then the cell gets the extra error, and there is no need to do the following steps. This covers case 2 in figure 3.9 and is probably in most cases the one used;
2. Otherwise, look if a corner point of the refinement area is in the cell. If this is true then the cell gets the extra error, and there is no need to do the following steps. This covers case 3 and case 4 in figure 3.9;

- Otherwise, look at the cell as a circle and determine the centre of the circle. If the distance from the centre to one of the sides of the refinement area is smaller than the radius of the circle, it should get the refinement error. This covers case 5 and case 6, which will occur when there is a very thin refinement line or in the first refinement steps, when the cells are still large compared to the refinement fields.

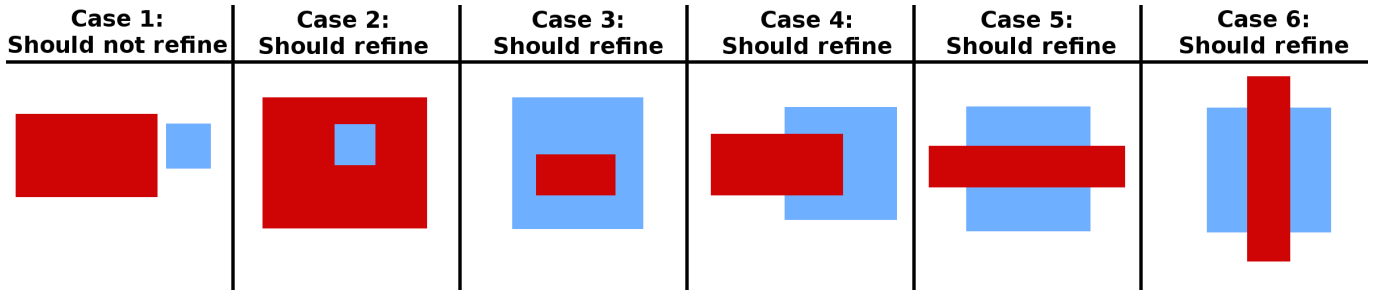


Figure 3.9: Shows six possible cases for the configuration of the area to add error (the rectangles in red) and the cell in question (the blue squares).

- **Initial temperature:** This allows the user to increase or decrease the initial temperature locally.
- **Composition:** This allows the user to change the composition within the defined area.

### 3.3.4 Converged Relative Residual adaptations

The Converged Relative Residual adaptations implement a new stopping criterion for the nonlinear iterations, called the Converged Relative Residual (CRR) criterion. The default stopping criterion is, as explained in section 3.1.5.2, based on a relative residual. This stopping criterion builds on this relative residual, of which a typical behavoir is shown in Fig. 3.10. The standart stopping criterion stops when the relative residual becomes lower then a fixed value. This may become problematic when the level the relative residual converges too changes significantly within a simulation. The CRR method determines whether the relative residual has converged and its value does not change within a certain tolerance over a few nonlinear iterations. It also tries to identify so called overshoots and uses the average of the relative residual values before and after the overshoot instead of the overshoot value.

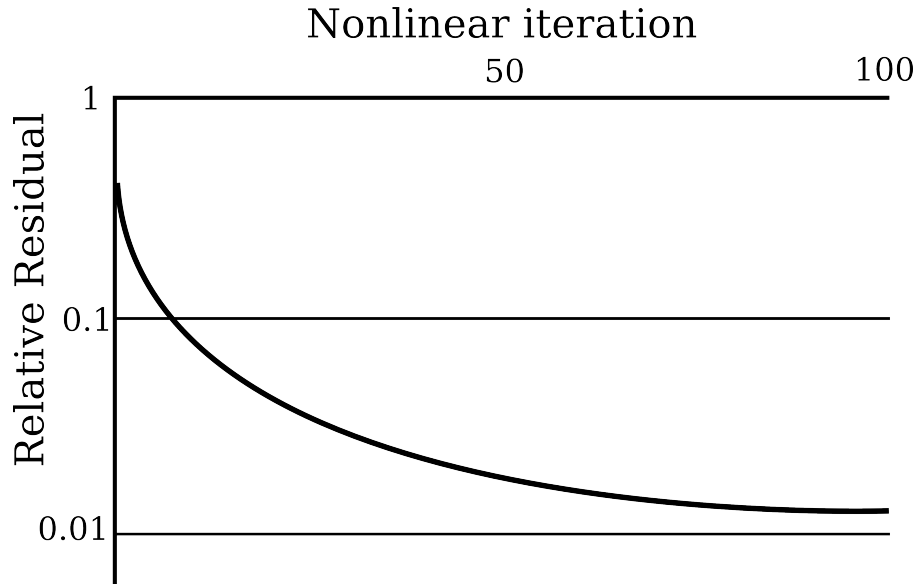


Figure 3.10: A schematic example of the behavoir of the relative residual with increasing nonlinear iterations.

An overshoot is defined here as a relative residual value which, based on the previous relative residual values, breaks the pattern by becoming very large, and at the next timestep return within the expected pattern.

The cause of these overshoots is unknown, but because they are only events limited to one iteration, and are always discovered two iterations after it occurred, they should not prevent the criterion from stopping the nonlinear iterations. Because the residual is always calculated for the previous solution, there is currently no way to determine if the last iteration was a overshoot.

To determine if the relative residual has converged, first a vector, which is by default length 5, is initiated with zero values, to store the relative residual values. Secondly a vector (hereafter called the change vector), with the same size, is initiated with minus the maximum change value, set by the user, to store the percentage of change of the log value of the relative residuals. If the average of the values in this vector becomes lower than a user set tolerance, for three times in a row, the nonlinear iterations are stopped.

Overshoots can be dealt with in two ways in this plugin. The first way is to simply limit the change vector values to a certain upper and under limit. The second approach is to actively identify overshoots and 'ignore' them in the change vector. Overshoots are identified by looking at the two previous relative residuals and the current relative residual. If the previous relative residual has changed more than 25%, compared to the relative residual two iterations ago, and the current relative residual is within 10% of the relative residual two iterations ago, the previous relative residual is considered an overshoot. The previous relative residual is then recalculated, based on the average of the relative residual two iterations ago, and the current relative residual. Based on the new values, the change vector is also updated. If before and/or during the overshoot iteration, the criterion was reached, then the counter for the amount of times the criterion is reached, is set accordingly.

It is also possible to set a minimum for the relative residual, which must be reached before the CRR criterion is allowed to stop the nonlinear iterations.

### 3.3.5 Initial fraction adaptations

The initial fraction adaptations enable the use of different refinement fractions for the IRS and for the timesteps. This allows for building a fine grid (high refinement fraction) at the start of the model, and then let the grid over the following timestep only change when it is really necessary (low refinement and coarsening fractions).

### 3.3.6 Maximum timestep adaptations

The maximum timestep adaptations allow the user to set a maximum timestep. This is necessary when the CFL condition allows for too large timesteps, causing the solver to not converge.

### 3.3.7 Line of tracers plugin and adaptations

The line of tracer plugin, together with some adaptions to the code, allow to create a horizontal (2D) line of passive tracers at a certain elevation. The tracers are positioned at an equal distance from each other. It is possible to limit the horizontal extent with a minimum and maximum x-position. This can be useful to track surfaces.

If tracers fall exactly on the boundary of two subdomains of the parallelisation (see section 3.1.2), the tracer is created twice. This is not a desired behaviour. To greatly reduce the chance of tracers being created exactly on a cell boundary which is also a boundary between two subdomains of the parallelisation, a very small number is added to the x position.

### 3.3.8 Stokes iterations adaptations

The stokes iterations adaptations prevent the nonlinear iterations from continuing when the stokes iterations become zero. If the stokes solver does not resolve the equations based on the updated matrix  $\mathbf{A}$ , then the

nonlinear iterations will only consume time without getting nearer to the real solution. It must be noted that if this happens a lot, one should consider making the linear solver tolerance for the Stokes solver stricter.

### 3.3.9 IRS increasing maximum nonlinear iterations adaptations

The IRS increasing maximum nonlinear iterations adaptations, which are only used in section 4.5.1, gradually increase the maximum nonlinear iterations ( $\tau$ ) according to Eq. (3.32). In each subsequent refinement step of the IRS, more nonlinear iterations are allowed.

$$\tau = \tau_{initial} \left( \frac{(pre\_refinement\_step + 1)}{(initial\_adaptive\_refinement + 1)} \right)^2 \quad (3.32)$$

### 3.3.10 Visualisation of normal deviatoric stress plugin

The visualisation of normal deviatoric stress plugin calculates the normal components of the stress deviator tensor ( $\sigma_x, \sigma_y, \sigma_z$ ) as stated in Eq. (3.33). The values of  $\sigma_x, \sigma_y$  and  $\sigma_z$  are then stored in a vector. Equation (3.33) is a simplification of the full formula, Eq. (3.34) (Schubert et al., 2001), where the  $\frac{\delta u_k}{\delta x_k}$  term becomes zero, because the model is incompressible. This plugin is intended to determine whether the system at a certain location is in a compressional or tensional regime in the x, y and z direction.

$$\sigma' = 2\eta\dot{\epsilon} \quad (3.33)$$

$$\sigma'_{ij} = 2\eta\dot{\epsilon}_{ij} - \frac{2}{3}\eta\dot{\epsilon}_{kk}\delta_{ij} = \eta\left(\frac{\delta u_i}{\delta x_j} + \frac{\delta u_j}{\delta x_i} + \frac{2}{3}\delta_{ij}\frac{\delta u_k}{\delta x_k}\right) \quad (3.34)$$

### 3.3.11 Extra output adaptations

The extra output adaptations provide extra information in the redirected screen output of ASPECT. This contains information on timing for the IRS, the residual per nonlinear iteration, nonlinear iteration number before the output of the nonlinear iteration and information about the CRR test, if used.

# Chapter 4

## General subduction modelling

### 4.1 Introduction

In this chapter all experiments with the plugins and adaptations are presented and discussed. All experiments use at least the general subduction plugin for composition, the general subduction plugin for temperature , the Stokes iteration adaptations and the extra ouput adaptations. All models also use use the parameters described in Section 4.1.1, unless explicitly stated otherwise.

#### 4.1.1 General setup of the system

All the models have a height of 760 km and a horizontal length of 1600 km, except for the general subduction models in Section 4.2 which have a horizontal length of 1000 km. The physical properties used, are shown in Table 4.1. The surface is set at 660 km from the bottom of the model. The use of these dimensions in this plugin means that the top 100 km is assigned a sticky air layer (see Section 3.3.1). The use of a sticky air layer of 100 km thickness was based on Crameri et al. (2012) and Hillebrand et al. (subm). Although our setups differ from those setups in some respects significantly, the 100 km of the sticky air layer, in combination with the top boundary being open (see Section 4.2) and a viscosity difference between the air and surface of five orders of magnitude, is taken to be a safe thickness for this layer.

#### 4.1.2 Boundary conditions

The temperature and composition boundary conditions use the initial temperature and initial composition at the boundaries, respectively, as boundary conditions. The velocity boundary conditions are more complicated. The top boundary is open for in- and outflow, the bottom boundary is free slip and the side boundaries can be set in the air and lithosphere to have a horizontal in- or outflow which is then compensated by an in- or outflow in the mantle (see Fig. 4.1). This compensation can be on the same side as the inflow, or on the other side. The vertical velocity on the side boundaries is always zero. Furthermore, it is possible to add an extra mantle flow component to the boundary part in the mantle.

### 4.2 General subduction modelling

This experiment is set up to test the basic (temperature, composition, rheology and velocity) plugins, adaptations and parameters in a subduction setting. Special focus is on the testing of the advection in the model. Therefore plate velocities have been chosen to represent the geological end members of plate velocities.

| Property (units)                              | Mantle      | subd. crust | ovr. crust | st. air  |
|---|-------------|-------------|------------|----------|
| Angle of internal friction ( $^{\circ}$ )     | 30          | 30          | 30         | 30       |
| Cohesion (MPa)                                | 20          | 20          | 20         | 20       |
| Heat capacity (JK $^{-1}$ )                   | 1e3         | 1e3         | 1e3        | 1e1      |
| Reference density (kgm $^{-3}$ )              | 3300        | 2900        | 2900       | 1        |
| Thermal conductivity (Wm $^{-1}K^{-1}$ )      | 4           | 4           | 4          | 10       |
| Dislocation prefactor (Pa $^{-n}s^{-1}$ )     | 3.12504e-14 | 1.1e-28     | 1.1e-28    | 1e-19    |
| Disl. activation energy (kJ mol $^{-1}$ )     | 430         | 223         | 223        | 0        |
| Disl. activation volume (m $^3$ mol $^{-1}$ ) | 15e-6       | 0           | 0          | 0        |
| Disl. constant coefficient $\nu$              | 1           | 1           | 1          | 1        |
| Diffusion prefactor (Pa $^{-n}s^{-1}$ )       | 1.92e-11    | 1.92e-11    | 1.92e-11   | 1.92e-11 |
| Diff. activation energy (J mol $^{-1}$ )      | 335e3       | 335e3       | 335e3      | 335e3    |
| Diff. activation volume (m $^3$ mol $^{-1}$ ) | 4.0e-6      | 4.0e-6      | 4.0e-6     | 4.0e-6   |
| Stress exponent for dislocation ( $n$ )       | 3           | 4           | 4          | 1        |
| Thermal expansion coefficient (K $^{-1}$ )    |             | 3e-5        |            |          |
| T <sub>pot</sub> slab (K)                     |             | 1553.0      |            |          |
| T <sub>pot</sub> mantle (K)                   |             | 1600.0      |            |          |
| Radius smoothing circle (km)                  |             | 750         |            |          |

Table 4.1: Table of physical properties used in the models. Subd. stands for subducting, ovr., stands for overriding and st. stand for sticky.

#### 4.2.1 Setup

The model has a subducting and the overriding lithosphere with a thickness of 80 km, of which the upper 10 km is crust. The subducting plate has been subducted for 76 km and has a dip of 30 degree. The plates are pushed from the left and the right side with a speed of 10 cm/year and 5 cm/year, respectively. The mantle velocity is 20 cm/year, either from the left or right direction.

#### 4.2.2 General subduction modelling results

Figure 4.2 shows the results of a 1.25 Myr simulation time for the model with the mantle flow from right to left. Figure 4.2a shows the initial viscosity field, the temperature isotherms in white with their respective temperatures on the left side, and the purple 0.5 isocontour for the crust compositions.

A few features are clearly visible in Fig. 4.2. Firstly, the building of topography. Directly after the first few timesteps, the overriding plate rises, while the subducting plate descends near the subduction zone. The creation of topography can also be seen in figure Fig. 4.3, where the surface can be more accurately seen by the density difference. Secondly, the plasticity component of the rheology plugin described in section 3.2 is creating shear-bands at locations marked with an A in Fig. 4.2. A1 in Fig. 4.2 shows shear-bands created by the extension needed to force the plate to bend, while the shear-bands at A2 in Fig. 4.2 are created by compression from the collision of the overriding plate with the subducting plate. It can be seen that at locations pointed out by C and D a chaotic pattern appears during the simulation. This happens at locations where at least some stress is expected. It is not clear what causes this chaotic pattern in the viscosity, and it might be a numerical problem such as the changing of grid resolution, or a lack of grid resolution, instead of a physical feature. Furthermore, the subduction channel, which is very thin, in these models is weak enough to allow for subduction, without the need to introduce an artificial weak zone. The subduction channel is kept weak by the nonlinear rheology, which decreases the viscosity when stress becomes high. Lastly, B in Fig. 4.2 shows the progression of the initial artificial bend in the subduction system. This bend is still clearly visible after 1.25 Myr of simulation.

In figure 4.3, where the density and isotherms are shown, three important observations can be made. The first observation is that the mantle flow only strongly influences the temperature field at the most deep part

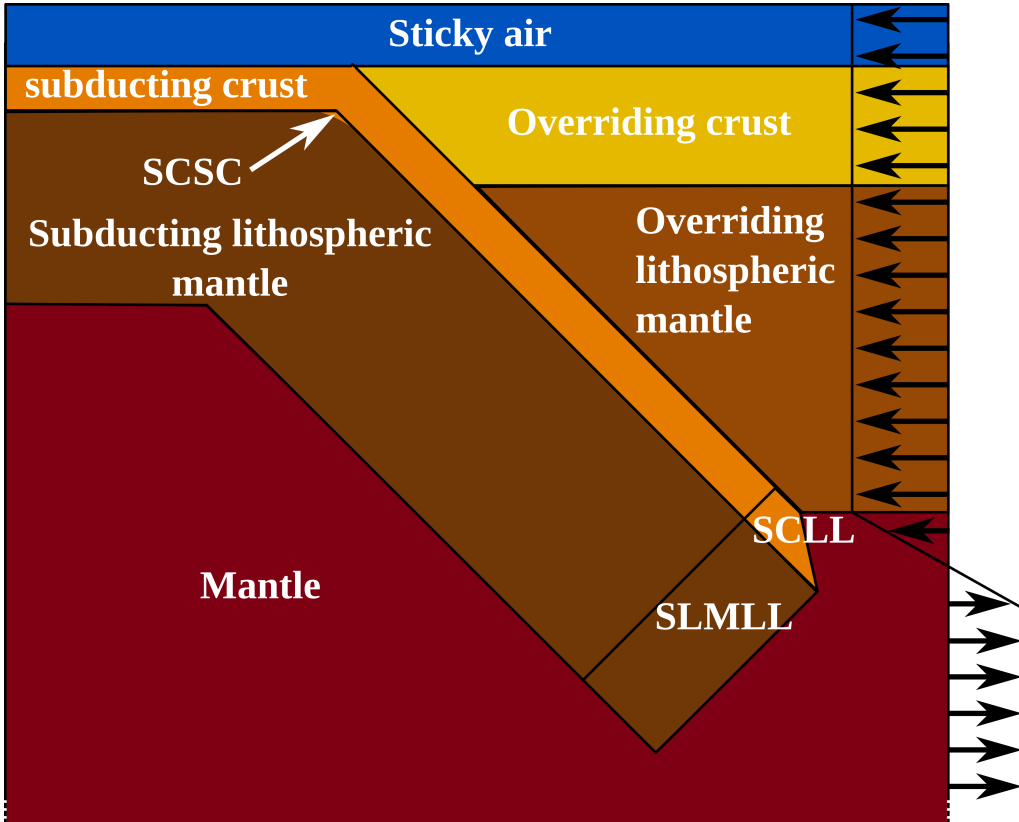


Figure 4.1: A schematic figure for the setup of the system. SCSC, SCLL and SCMLL represent Subducted Crust added by the Smoothing Circle (see section 3.3.1), Subducted Crust if the subducting Lithosphere is so Long that it comes out under the lithosphere, and Subducting Lithospheric Mantle for a Long Lithosphere respectively. The black arrows illustrate the in- and outflow setup on the right boundary for a overriding plate which is pushed in. The plate can also be pulled out, leading to a reversed pattern for the arrows, and it can be applied to both sides.

of the slab (see A at Fig. 4.3). The second observation is the accumulation of crustal material at a depth of about 55 km. This coincides with the lithosphere-asthenosphere transition. The last observation is that the temperature is elevated on the surface at the the subduction zone (C in Fig. 4.3).

### 4.3 Surface study with passive tracers

This experiment is set up to test whether the compositions in combination with the sticky air method are able to correctly create a surface which can be tracked. For this purpose the implemented passive line of tracers plugin and adaptations are used. The initial line, which contains 38000 tracers, is set at an elevation of 660 km from the bottom, which coincides with the initial surface elevation. The evolution of these tracers is compared with the the top contour line of the crustal composition at the value 0.5.

The model has a subducting plate with a lithospheric thickness of 80 km and a crust of 5 km. The overriding plate has a lithospheric thickness of 100 km and a crust of 6 km. The model starts with an initial subducted plate of 100 km at 25 degree dip.

These experiments, of which an example is shown in Fig. 4.4, show that that the 0.5 contour line and the position of the tracers follow the same trends in the elevation, and that they deviate only a fraction of a grid element from each other. However, the computation of the tracers did cost significantly more computational time.

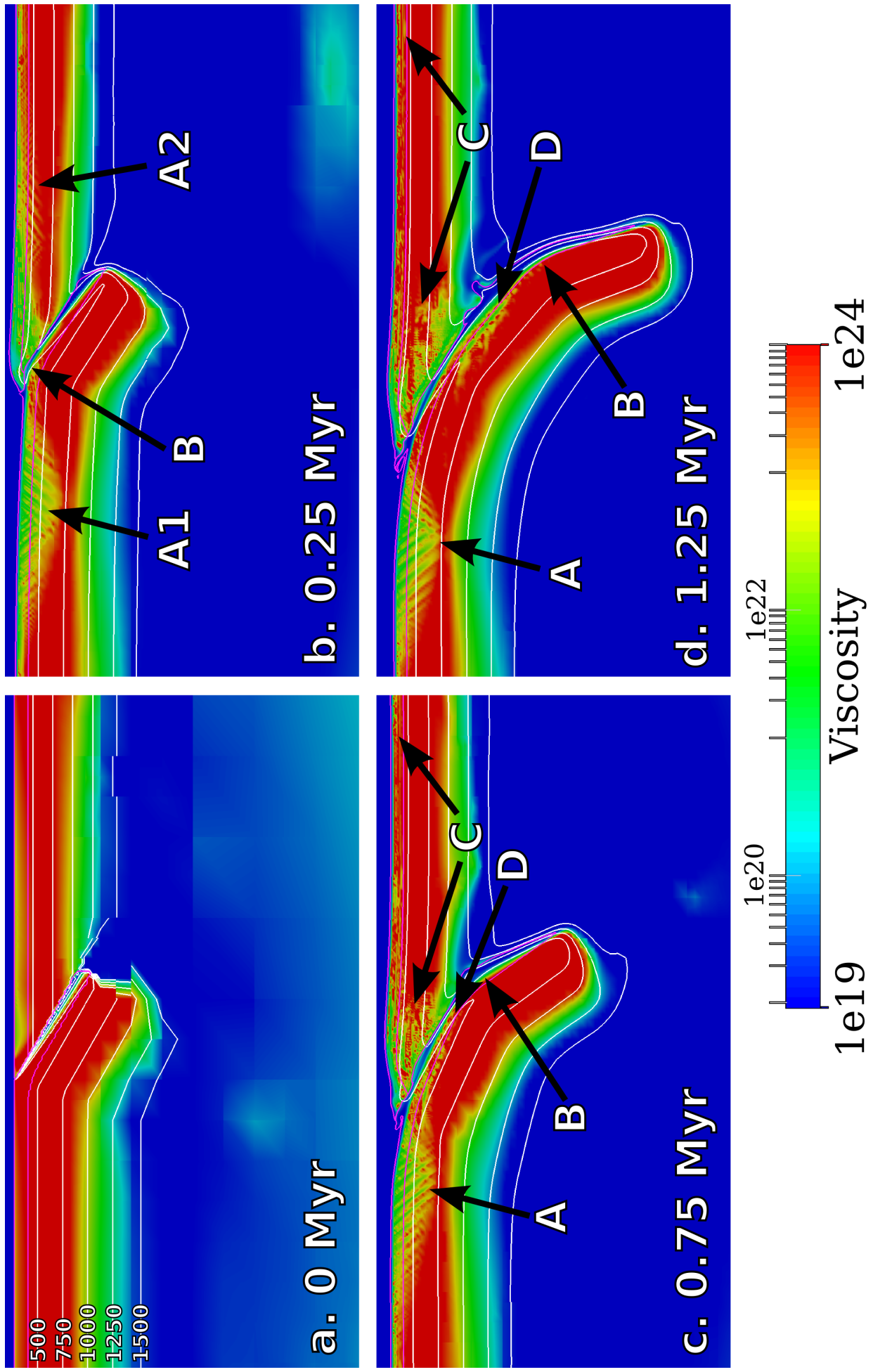


Figure 4.2: A zoom on the subduction zone for the results for the general subduction modelling with the mantle flow from left to right for different times in the simulation. The white lines are isotherms, and the purple line is the 0.5 isocountour for the crust compositions. A shows clear shear-bands, B shows the progression of the artificial bend in the slab and C and D show the locations of chaotic viscosity behaviour.

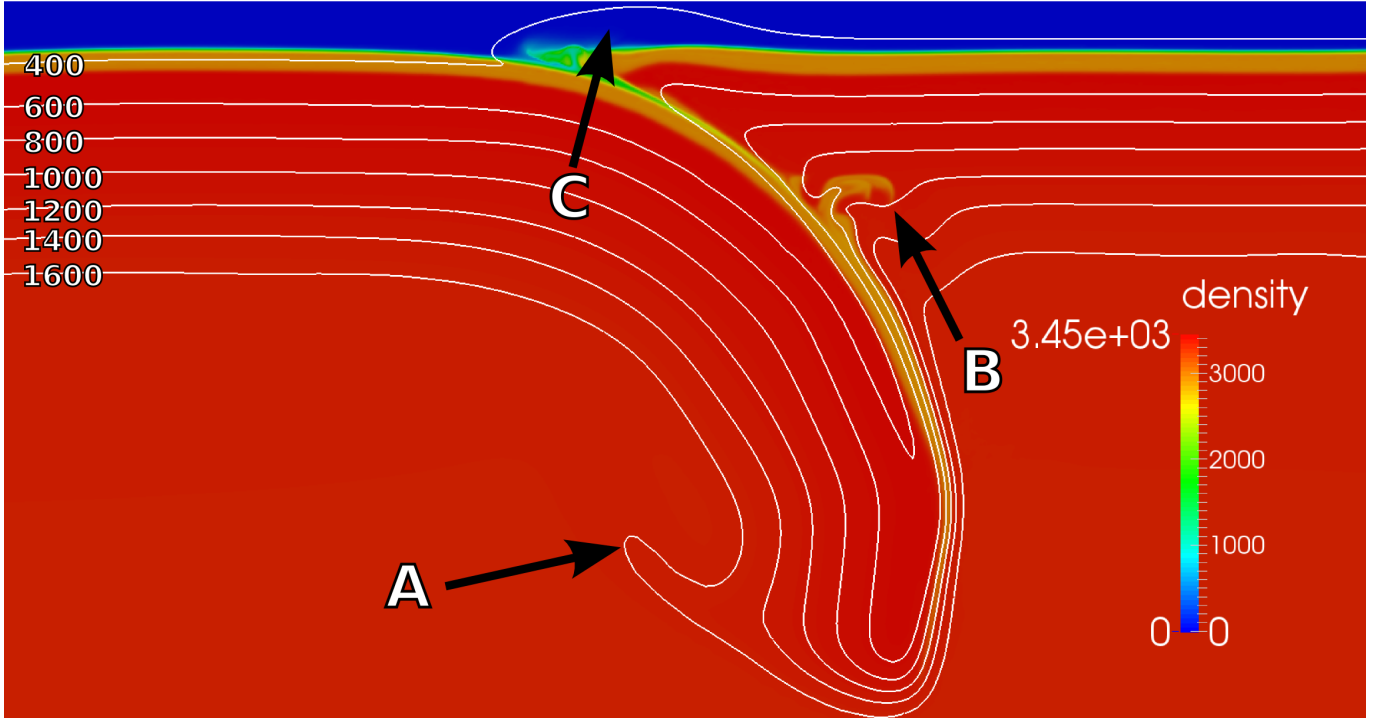


Figure 4.3: A zoom on the subduction zone for the results for the general subduction modelling with the mantle flow from right to left for the density at 1.85 Myr simulation time. The white lines indicate the isolterms for 400K to 1600K, with jumps of 200K

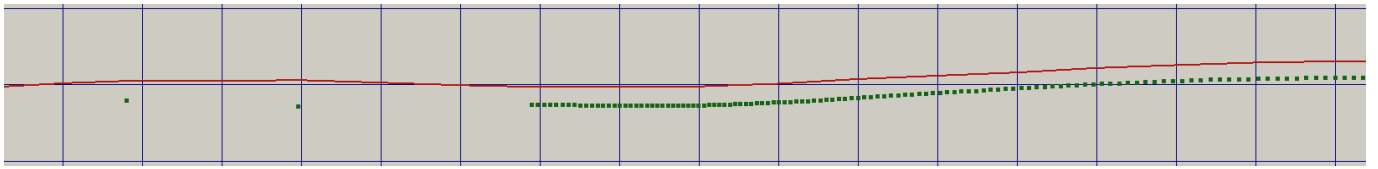


Figure 4.4: A zoom on the location of the surface. The blue lines show the elements, which are 740 by 740 meters. The red line indicates the 0.5 isocontour of the crustal composition, and the green dots represent the tracers.

## 4.4 Tolerance Study

### 4.4.1 Setup

Both the linear Stokes solver and the nonlinear iterations contain a tolerance which can be set. Furthermore a maximum amount of nonlinear iterations can be set. The experiments in the tolerance study try to determine what the influence of these parameters is on both the solution and the time to calculate the solution. The default value in ASPECT for the Stokes solver ( $\omega$ ) is 1e-7, and the nonlinear tolerance ( $\psi$ ) is by default set to 1e-5.

The model has a subducting lithosphere which is 80 km thick, of which the upper 5 km is crust and a overriding lithosphere which is 150 km thick of which the upper 38 km is crust. Two weak zones (forced lower viscosity, see Fig. 4.5) have been placed in the overriding plate with each a length of 50 km and dipping to the right at an angle of 30 degrees. The subducting plate is initially subducted for 550 km at a dip of 30 degrees. The system is not forced form the sides.

For this study several simulations have been carried out, as shown in table 4.2. They are named according to the amount of nonlinear iterations, the Stokes solver tolerance and the nonlinear tolerance which have been used in the model runs.

| #  | name        | Max nonlinear iterations | Stokes solver tolerance | Nonlinear solver tolerance |
|----|-------------|--------------------------|-------------------------|----------------------------|
| 1  | 15nl-5t-2bt | 15                       | 1e-5                    | 1e-2                       |
| 2  | 15nl-7t-2bt | 15                       | 1e-7                    | 1e-2                       |
| 3  | 30nl-4t-2bt | 30                       | 1e-4                    | 1e-2                       |
| 4  | 30nl-5t-2bt | 30                       | 1e-5                    | 1e-2                       |
| 5  | 30nl-6t-2bt | 30                       | 1e-6                    | 1e-2                       |
| 6  | 30nl-7t-2bt | 30                       | 1e-7                    | 1e-2                       |
| 7  | 30nl-8t-2bt | 30                       | 1e-8                    | 1e-2                       |
| 8  | 60nl-5t-2bt | 60                       | 1e-5                    | 1e-2                       |
| 9  | 60nl-7t-2bt | 60                       | 1e-7                    | 1e-2                       |
| 10 | 90nl-5t-2bt | 90                       | 1e-5                    | 1e-2                       |
| 11 | 90nl-7t-2bt | 90                       | 1e-7                    | 1e-2                       |
| 12 | 90nl-5t-3bt | 90                       | 1e-5                    | 1e-3                       |
| 13 | 90nl-7t-3bt | 90                       | 1e-7                    | 1e-3                       |

Table 4.2: Table of the model parameters.

Without an analytical solution it is hard to determine if one solution is more or less correct than an other solution. However, it can be assumed that if the tolerances are set to be stricter, and more nonlinear iterations are allowed, that the solution is more correct. The solutions are therefore compared to each other in this respect. In this comparison, the following factors will be taken into consideration:

1. **Simulation time:** look at the simulation time at a timestep. Because if solutions are the same, the timestep will also be the same.
2. **Vrms:** The root mean square of the velocity. The vrms is especially sensitive to large scale changes in the velocity field, even if they are small in magnitude.
3. **Vmax:** The maximum velocity. The vmax is more sensitive to small scale changes in the velocity field, because it is not smoothed by averaging.
4. **Total viscous dissipation:** The total viscous dissipation is a term for the energy generated by the friction of the flow which is transformed into heat. This factor also takes other factors into consideration besides velocity, such as viscosity and strain-rate.
5. **End relative residual:** The relative residual value of the last nonlinear iteration. If the relative residual is large, the system of equations is probably not well solved and therefore less correct. It must be noted that technically it is not the relative residual of the last iteration but of the penultimate iteration, because first the residual of the previous solve is calculated before resolving the model. The residual for the last nonlinear iteration is therefore never calculated.

#### 4.4.2 Results

**Simulation time** Figure 4.6 A shows the simulation time at several timesteps in different model runs. There is no significant difference in model runs at each timestep.

**The root mean square velocity** The Vrms in Figure 4.7A and 4.7B is more sensitive to the amount of maximum nonlinear iterations ( $\tau$ ) than to the Stokes solve tolerance at the first timestep. At later timesteps, especially 50 and 100 there is a significant difference between the model runs, but there is no clear correlation between the changing in parameters and the Vrms.

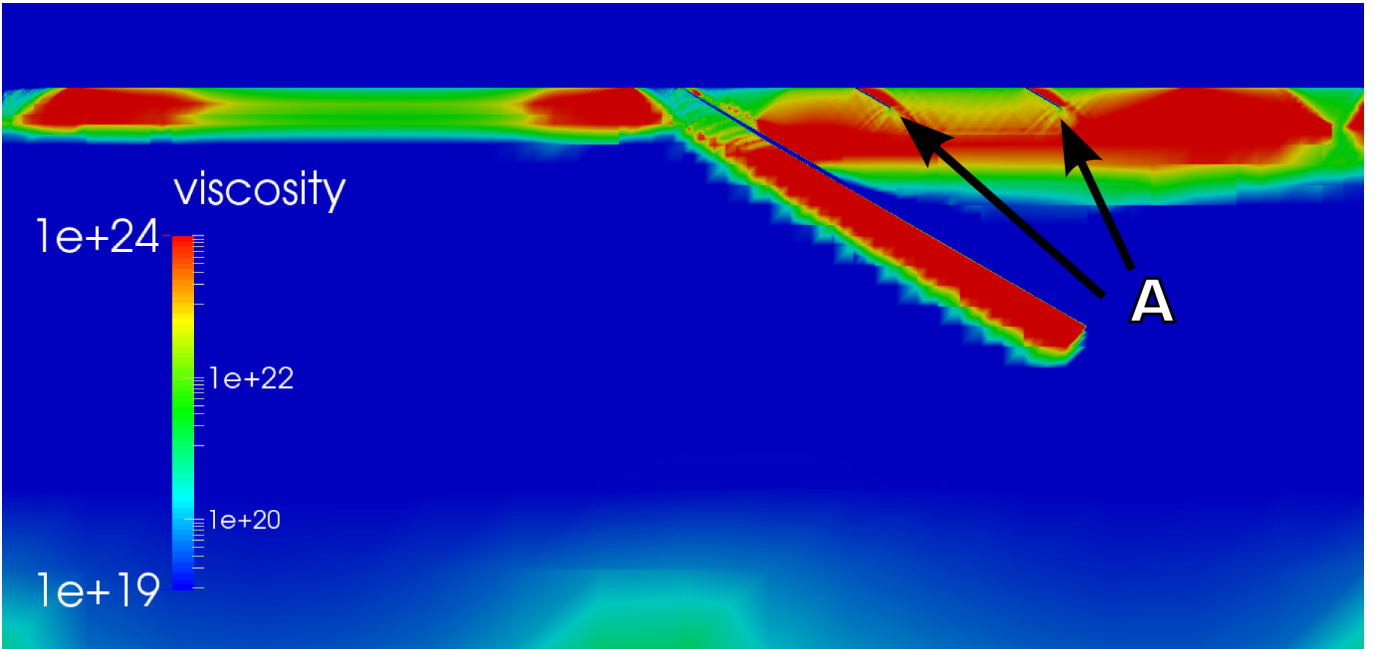


Figure 4.5: The setup for the viscosity after the IRS have solved the initial system. A indicates the prescribed weak zones.

**The maximum velocity** The Vmax in Figure 4.6B follows the same pattern as the Vrms for timestep one. For later timesteps the behaviour is also similar to the Vrms, where there is no clear correlation between the changing of parameters and the results.

**The total viscous dissipation** Although the general pattern for the first timestep of the total viscous dissipation shown in Fig. 4.7C is similar, the model runs 15nl t5 and t7 and 30nl t4 differ a bit from the other model runs which are very consistent. A greater deviation is shown in Fig. 4.7D, which shows for the model with a  $\omega$  of 1e-4 a very large deviation compared to the mean of the other models.

**The end relative residual** The end relative residual in the IRS and the first 15 timesteps is shown in Fig. 4.8A and 4.8B. They show a clear and direct correlation between the amount of nonlinear iterations used and the end relative residual of the timestep. This is especially the case for the IRS (below one). Although this also seems to be the case for the first timestep, the 60nl 5t model is an exception. When looked at in close detail, one sees that the end relative residual decreases steadily up to iteration 59 to 0.107525, but at iteration 60 rose to 0.469083. This is therefore seen as an overshoot (see section 3.3.4), which happened with the last nonlinear iteration.

After timestep one, it can be clearly seen that the relative residual for the solution with a  $\omega$  of 1e-4 deviates the most from the set  $\psi$  of 1e-2, followed by model run 15nl t5. It can also be seen that if a  $\psi$  of 1e-3 is set, it will not be reached within 90 nonlinear iterations for this setup. These patterns are even more clear in the later timestep in Fig. 4.8C and 4.8D.

**Run time** As can be seen in Fig. 4.9, the first order influence on the runtime is  $\omega$ . Changing  $\omega$  one order of magnitude can result in a drop or raise of 60 percent in runtime (see Fig. 4.9C), while the solution stays nearly the same up to a tolerance of 1e-5.

Increasing  $\tau$  from 30 to 60 takes with a  $\omega$  of 1e-7 about 20% more time (see Fig. 4.9C). Further increasing it to 90 nonlinear iterations hardly takes any extra time for the run with a  $\psi$  of 1e-2, especially in the long run. This can be explained by the fact that the  $\psi$  often, but not always, hit in this setup just before or after the 60th iteration. This is one of the reasons why it does not take that much more time for the

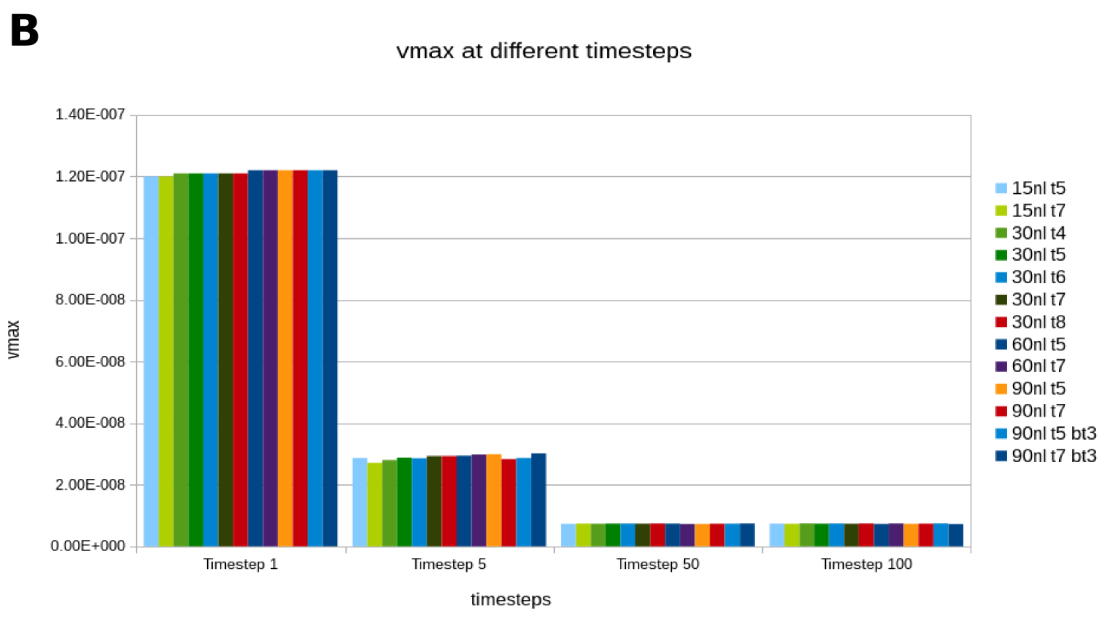
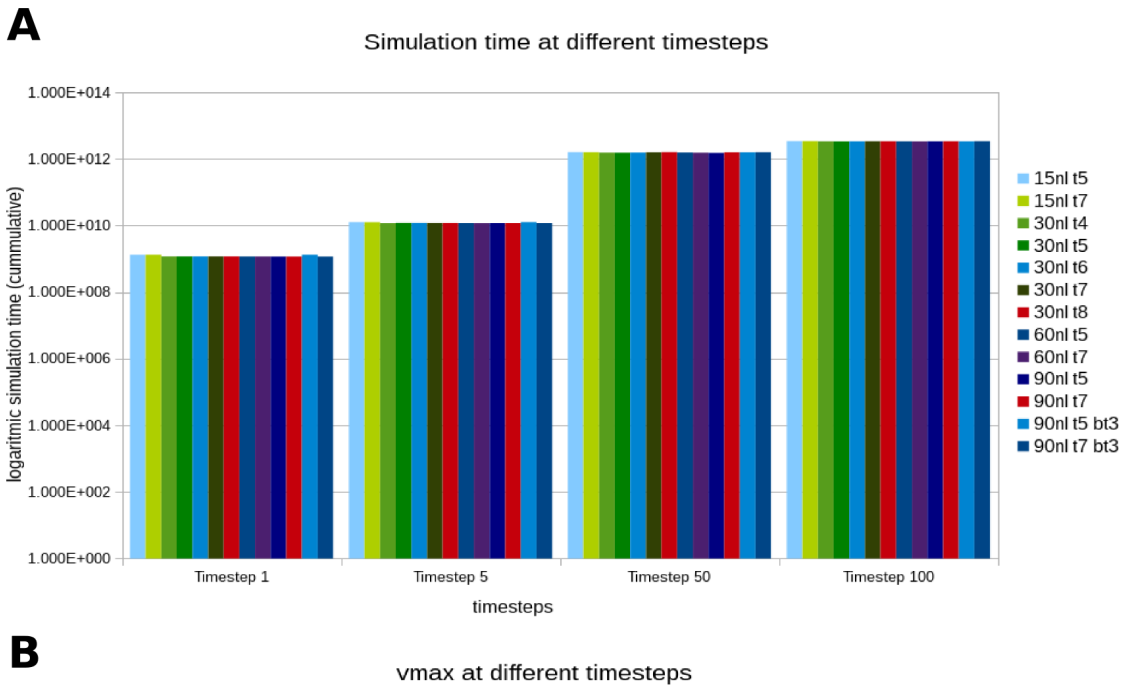


Figure 4.6: The different indicators for the different models at timesteps 1 ,5, 50 and 100. Figure A shows the simulation time.

models with a increased  $\tau$ . Another reason is that the first few iterations usually take a lot of time, while later iterations take less time. When  $\omega$  is set to 1e-5, the difference in runtime between a maximum of 30, 60 or 90 iterations practically disappears.

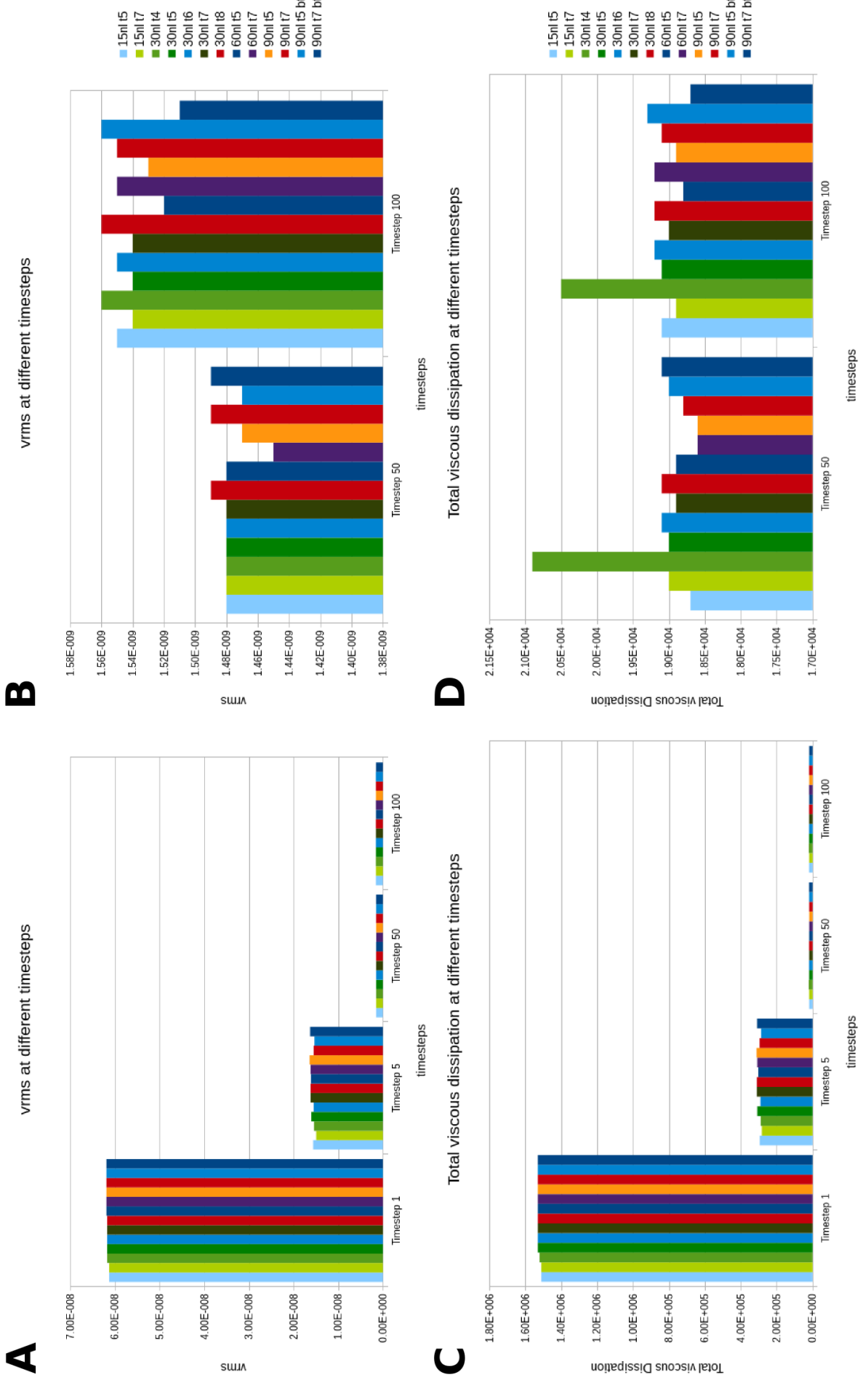


Figure 4.7: The different indicators for the different models at timesteps 1 ,5, 50 and 100. Figure A and B show the Vrms. Figure C and D show the total viscous dissipation.

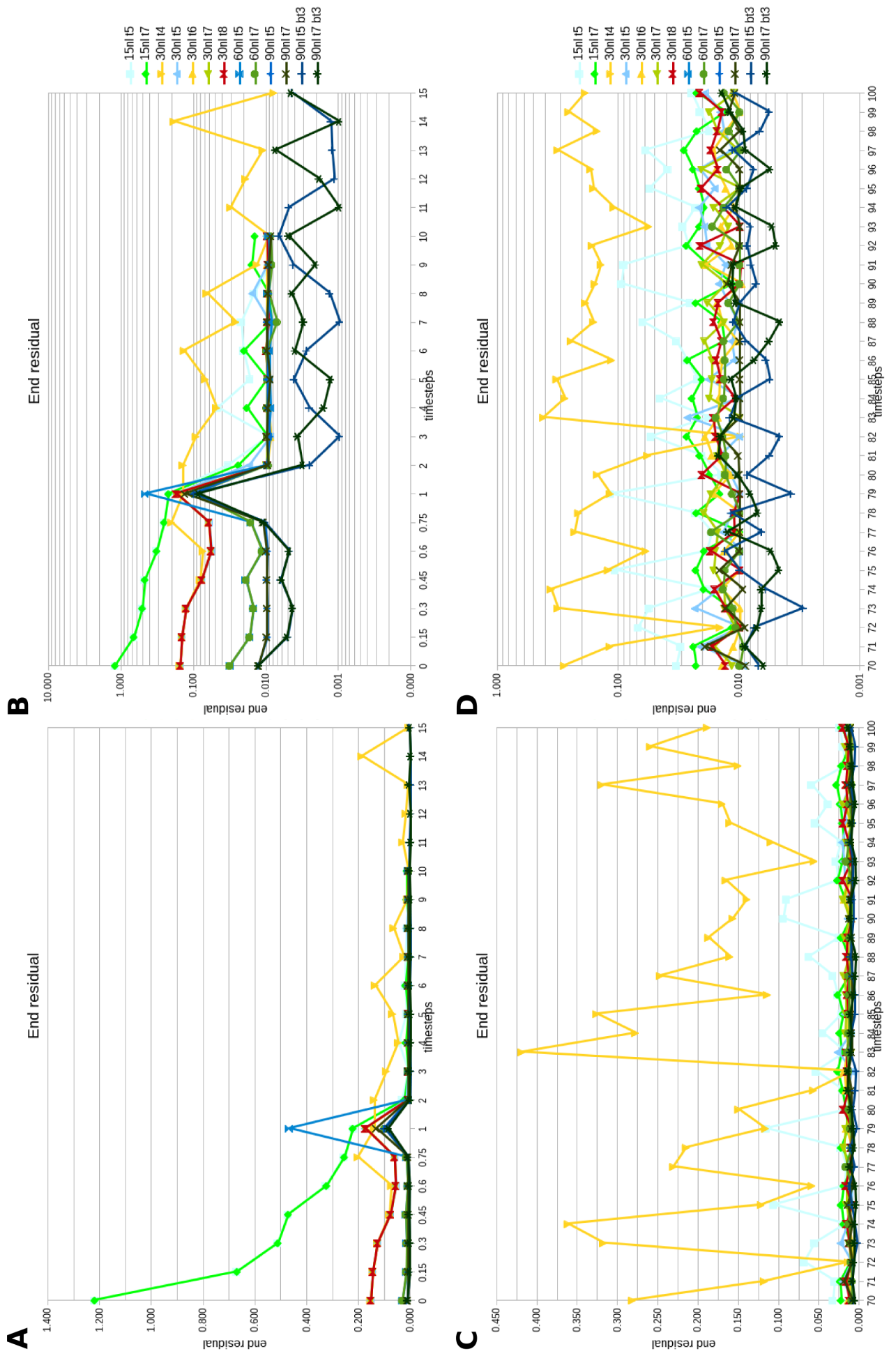


Figure 4.8: End residuals at different timesteps. Steps below zero are the IRS. A) Graph of the end residual from timestep 0 to timestep 10/15. B) Logarithmic version of graph A. C) Graph of end residual from timestep 70 to timestep 100. D) Logarithmic version of graph C.

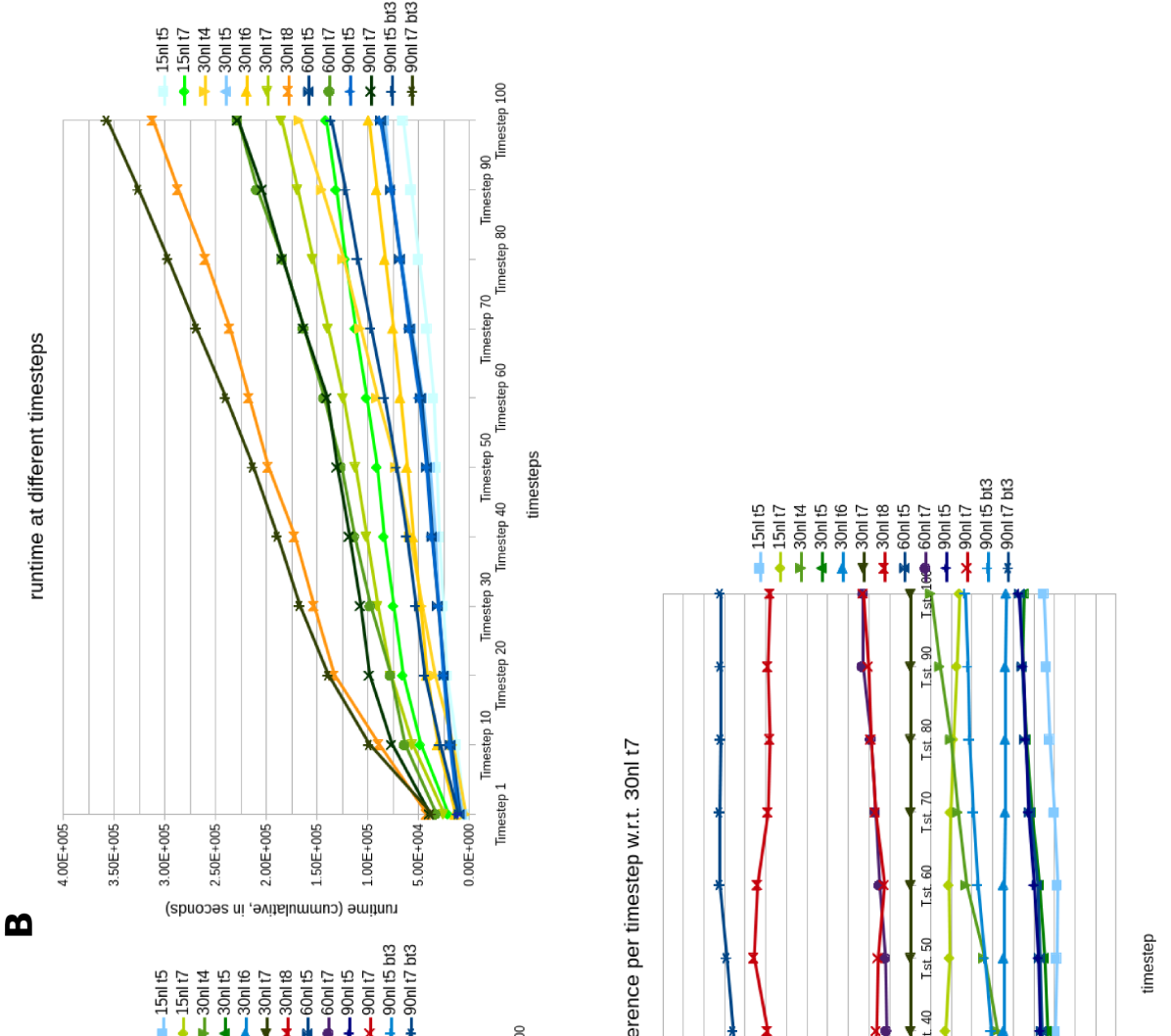
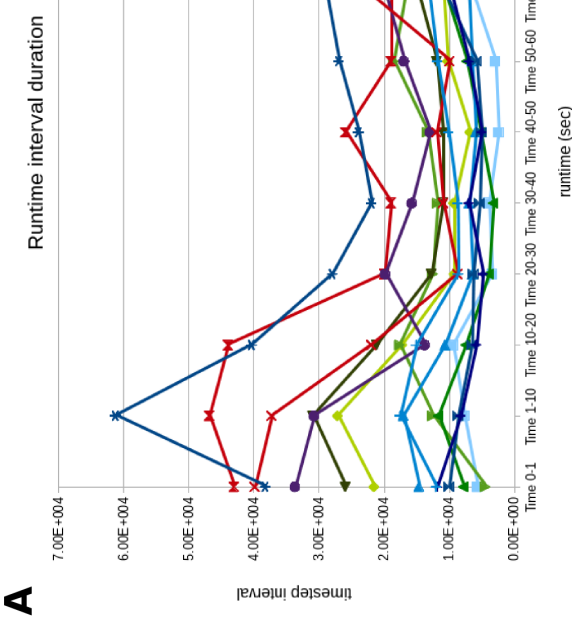


Figure 4.9: Runtimes for different models. The IRS are not shown. A) The time each interval of 10 timestep takes to run. B) Cumulative runtime of the different setups. C) The runtime difference per 10 timesteps with respect to model run 30nl t7.

## 4.5 Timing Study

The goal of the timing study is to investigate possibilities to make a case study type of model, discussed in Section 4.6, run faster. This model has a subducting plate with a lithospheric thickness of 100 km of which 7 km is crust. The overriding plate has a lithospheric thickness of 150 km, of which 38 km is crust. The plate has initially subducted for 76 km at a dip of 30 degree. The subducting plate is pushed with a speed of 1.667 cm/year. This value is based on van Hinsbergen et al. (2014), where it is stated that between 85 and 45 Ma, convergence rates were very low, and that it is unlikely that a subducting slab had been formed by 45 Ma below Iberia, and that the length of a northwest dipping slab below Sardinia at the inception of western Mediterranean rollback some 30 Ma may have been 250 km.

There are three parts to this study, which all use a  $\tau$  of 100 unless otherwise stated. The first part investigates the limiting of the IRS. This is investigated because it has been noticed that the IRS takes a significant amount of time and the IRS solution differs visually a lot from further timestep solutions. The second part investigates if it is better to push directly, or first let the model relax for a time. The third part investigates the behaviour of the residual. This last part will make use of the CRR adaptations.

The name of the model run always starts with the amount of nodes which have been used on the cluster followed by an 'n' (e.g. for six nodes '6n'). The 'nlt' stand for the non linear tolerance, of which the used value precedes this abbreviation. The 'df' stand for direct flow, which means that the lithosphere is directly pushed, and no relaxation time is allowed.

### 4.5.1 Limiting the IRS

This experiment tests whether limiting  $\tau$  during the IRS saves time without changing the solution. This might be possible, because the IRS before the last IRS are only used to build a grid. Although it is very important to have a good representative grid, it might not be required to have a perfectly solved system for the creation of this grid. The IRS increasing maximum nonlinear iterations adaptations (section 3.3.9) were used to test this assumption.

The results for two cases are shown in Fig. 4.10. It shows that the method used saves about 5% time in both cases. The difference in solution is not investigated, because the time saved with this method was not enough to be actually useful.

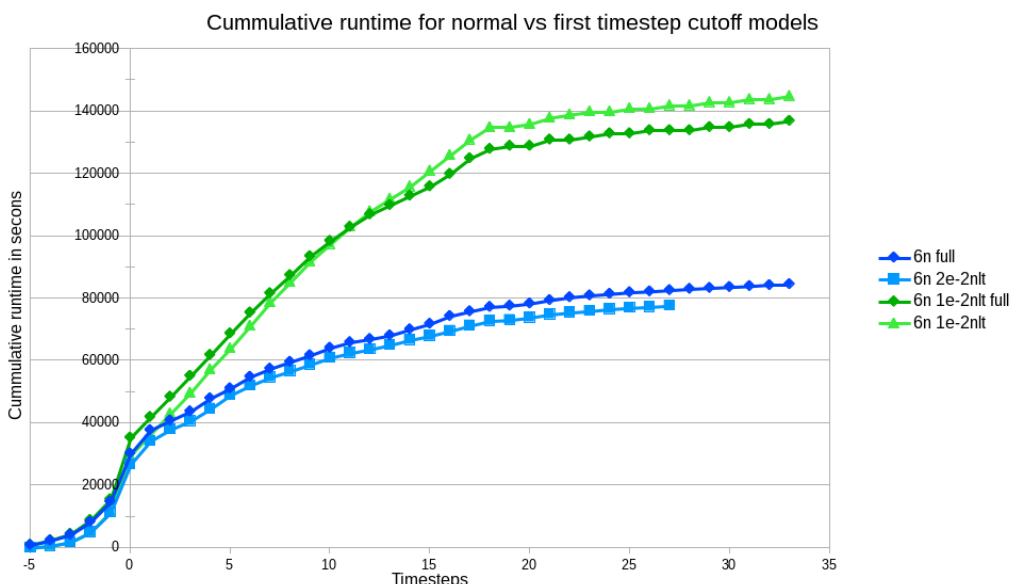


Figure 4.10: The timing results for normal (full) and limited nonlinear iterations for the IRS and 33 timesteps after.

#### 4.5.2 To relax or not to relax

When the setup of numerical models in the Earth Sciences is defined, it does not mean, and it is unlikely that the configuration is in perfect equilibrium. Therefore, it is sometimes needed to first let the model get into, or near to, an equilibrium, before enforcing for example velocity condition from the sides. This process is called relaxing of the model. In the previously described models, the system was first relaxed before the side velocity conditions where applied. This experiment is designed to investigate the effect of this relaxing. In this case a relaxing time of 2000 years has been used. The results are clear:

- The residual is two orders of magnitude lower in the direct flow models
- The direct flow models take less time

These two observations are of course linked. The link is that because of the lower residual, the cut off criterion is reached within less nonlinear iterations, and therefore take less time. It is with the current output of ASPECT not possible to say if the iterations themselves take less time, although making the adaptations should be trivial. The problem with less nonlinear iterations is that artifacts in the solution are not iterated out. It is therefore necessary to make  $\psi$  stricter. The results can be seen in Fig. 4.11. The outcome is that by allowing the flow directly, the relative residual can be significantly lower in about the same time. Because of this, the following models in this thesis will not use relaxing.

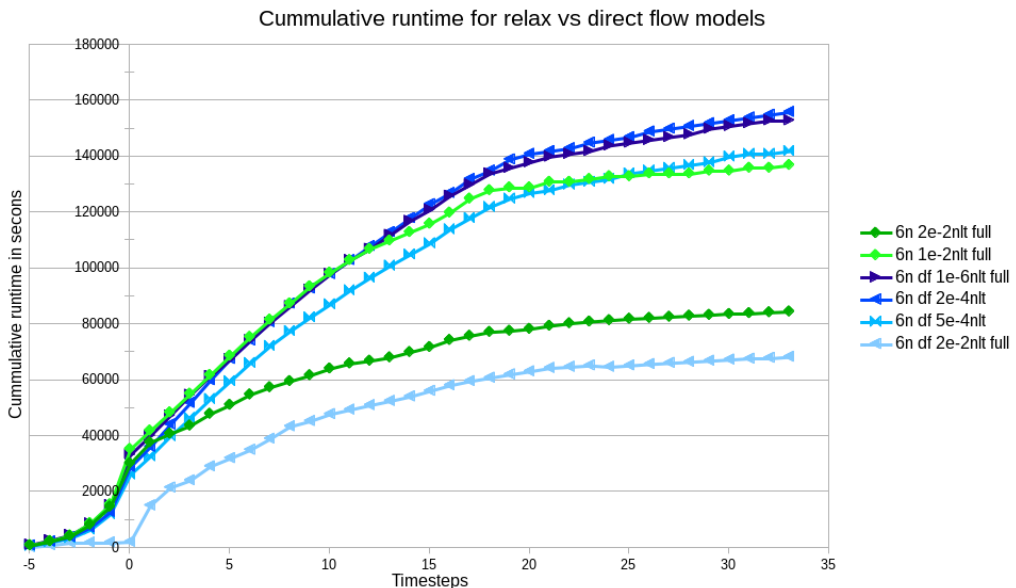


Figure 4.11: The timing results for normal (relaxing) in green and direct flow (df) models in blue.

#### 4.5.3 A relative residual study

These experiments are focused on investigating the behaviour of the relative residual. In addition, the experiments test the CRR adaptations. The results of a typical example are shown in Fig. 4.12. The following behaviour can be seen:

1. All of the IRS relative residual first increase before decreasing during the nonlinear iteration process. All timesteps, that is after the IRS, do not show this behaviour.
2. The first step of the IRS start to decrease at a constant rate after several iterations, while the other IRS decrease to a limit. Note that this limit does not always have to be the same.
3. In all the model runs, the -2 IRS has the tendency to strongly oscillate at the later nonlinear iterations.
4. All timesteps can have overshoots at nearly any point during the nonlinear iteration process.

5. The first timestep seems to converge really fast to a residual value which is very different to that of the other timestep.

The sharp increase in the relative residual during the IRS might have to do with that during the solving of the system, usually the two previous timesteps are used. This is for the IRS not possible, because there are no previous timesteps. This explanation might also be used for why the first timestep relative residual is behaving so differently, because it can only use the solution from the IRS, and not two timestep back.

The reason that the relative residual value converges to a certain value is not understood. But it is interpreted as that the solution does not change a lot anymore. The nonlinear iterations can therefore be stopped by the CRR method.

The oscillations at the end of the -2 IRS might be explained by the fact that the grid reaches a resolution at which it starts to resolve parts of the fine structure of the model and has a hard time to solve very accurately for these partially visible' structures. It must be strongly noted that this is only a theory, and that the precise nature of these oscillations is not known.

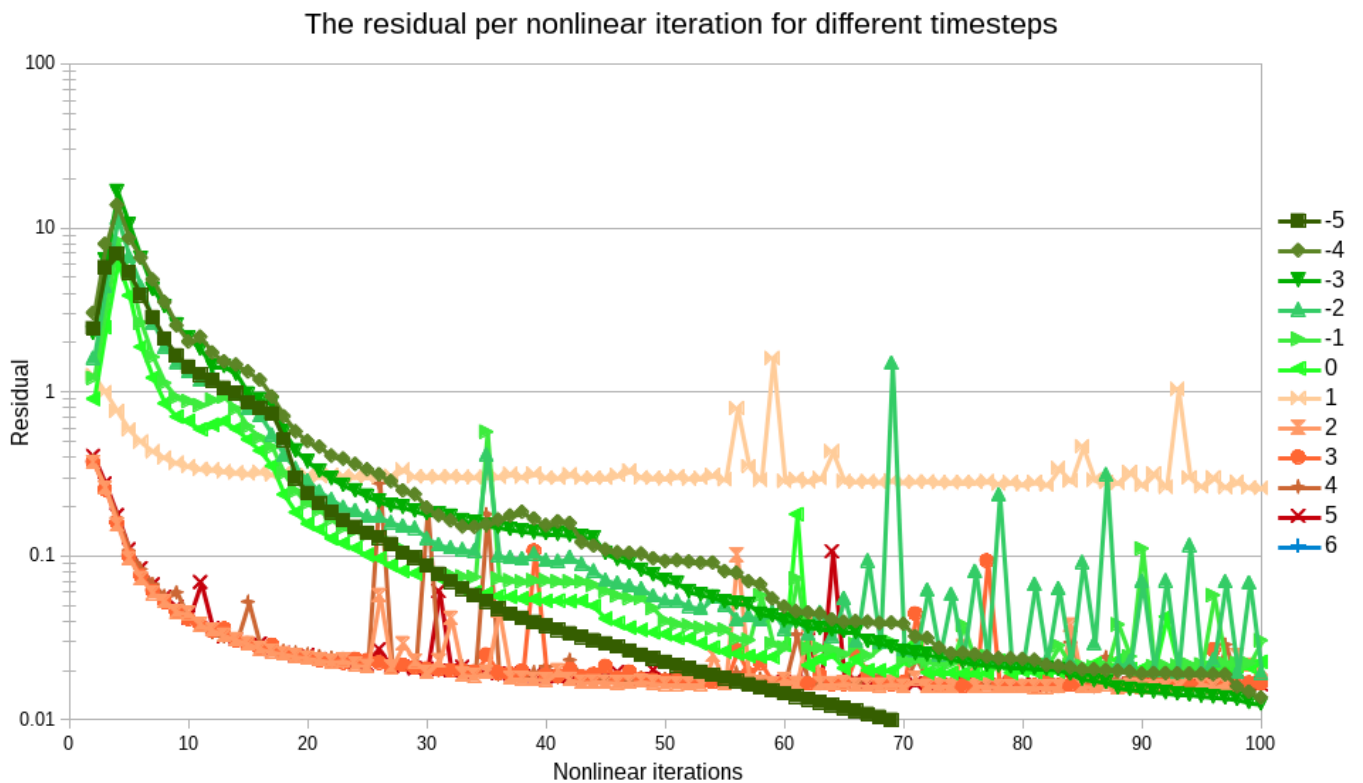


Figure 4.12: Example of the development of the residual for the IRS (-5 to 0) and the first 6 timesteps for one of the model runs.

## 4.6 Towards a Western Mediterranean case study

### 4.6.1 Geological setting

**Before 85 Ma** At 200 Ma, Iberia was part of the supercontinent Pangea (Handy et al., 2010; Vissers et al., 2013). During the breakup of Pangea in the Jurassic (200-140Ma), the Piemonte-Ligurian Ocean opened between Iberia and Adria/Africa (Frisch, 1979; Vissers et al., 2013) (see figure 4.13). Vissers et al. (2013) calculated that the extension in the Piemonte-Ligurian Ocean must have been about 450 km. Between 121 Ma and 83 Ma, it is unlikely that there was any convergence between Africa and Iberia according to van Hinsbergen et al. (2014). It is possible that there was even a small extension during this period. This is

supported by Faccenna et al. (2001a), who stated that after the rotation phase between 132 and 124 Ma, the rotation slowed down and was followed by translation from about 120 Ma till 85 Ma. The transform fault along which this occurred has now been subducted (van Hinsbergen et al., 2014).

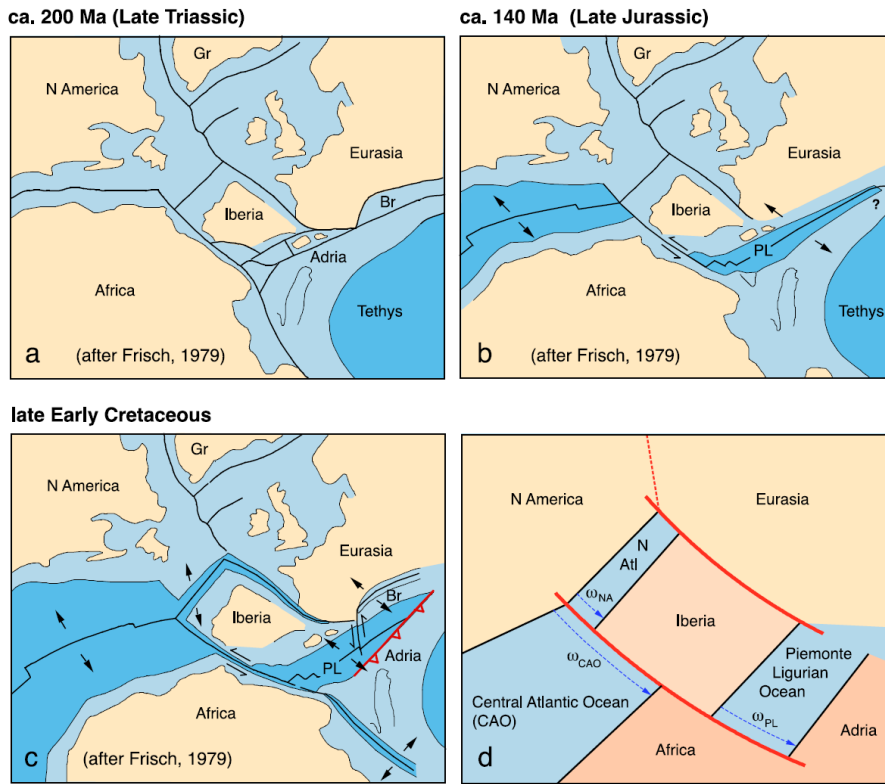


Figure 4.13: Geological setting from the Late Triassic (ca. 200 Ma) to the late Early Cretaceous (ca. 125 Ma) from Vissers et al. (2013).

**85 Ma - present** After 85 Ma convergence started between Iberia and Africa at a very slow rate (1-2 cm/year) (Faccenna et al., 2001a,b; Handy et al., 2010; van Hinsbergen et al., 2014). It is seen as unlikely that a subducting slab had formed before 45 Ma (van Hinsbergen et al., 2014).

Most of the Africa-Europe convergence occurred after 45 Ma (about 220 km) (van Hinsbergen et al., 2014). Due to the rotational nature of the convergence of Africa and Europe, the amount of convergence differed per location in the Mediterranean. Below Sardinia there may have been a slab of about 250 km, while near Gibraltar only a few tens of kilometres of convergence had occurred. However, it is unlikely that a well developed slab existed under Sardinia at 30 Ma (van Hinsbergen et al., 2014).

At 30 Ma rollback in the western Mediterranean was initiated. This rollback pulled Sardinia and Corsica from their original location near Iberia and Southern France (see figure 4.14). At around 15 Ma the rollback halted till 10 Ma, after which the rollback continued to the present situation. The reason for this halt in the rollback is still being debated. Since the details of the debate are not relevant for the current research, the reader is referred to Carminati et al. (2012) for more information about the different hypotheses on why the rollback halted.

#### 4.6.2 Setup

The goal of the models in this section is to simulate the subduction and rollback of the western Mediterranean region above the NBTZ (the red line in Fig. 4.14), with and without the weak zone. An attempt is made

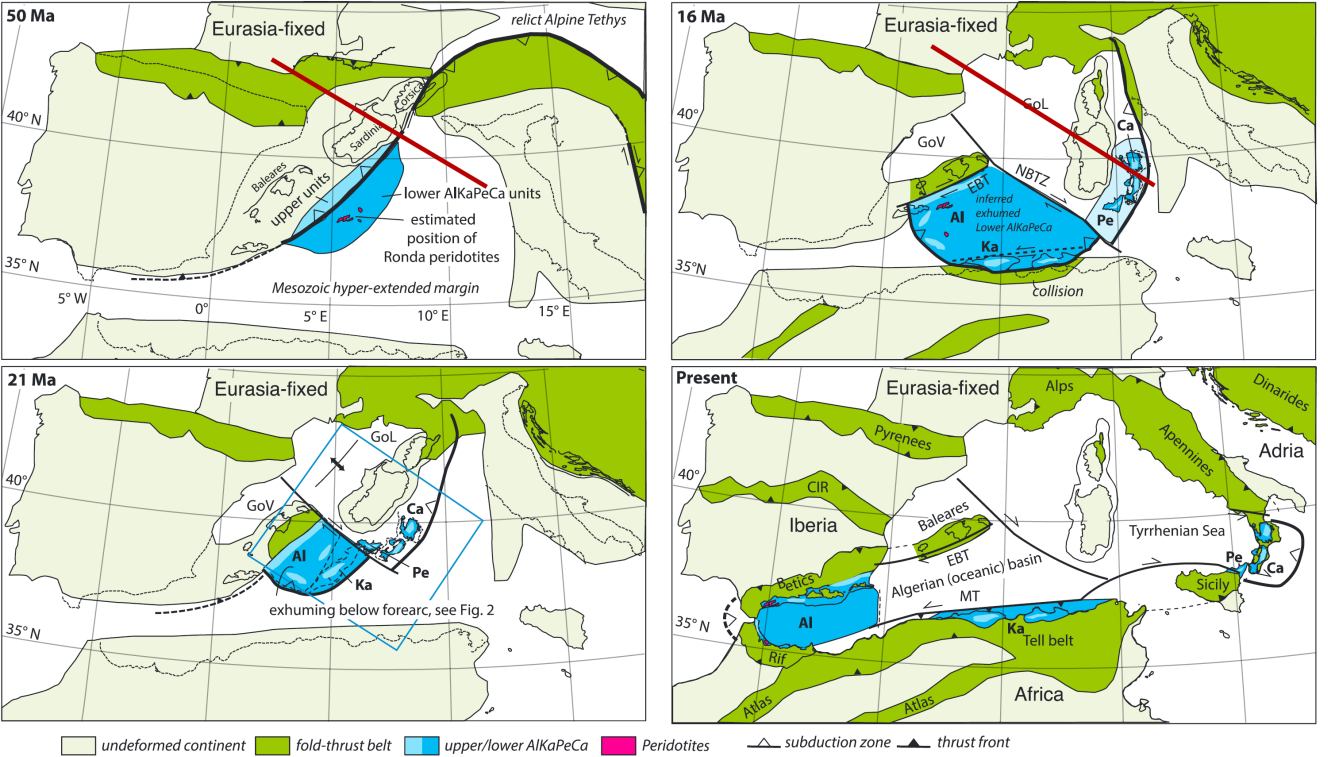


Figure 4.14: Geological setting from the start of faster convergence (ca. 45 Ma) to the present from van Hinsbergen et al. (2014). The red line indicates the location of the 2D section which is studied.

to investigate the role of a weak zone in the overriding lithosphere. To this end, a line from France/Spain, through Sardinia to Piermonte Ligurian Ocean is taken as the 2D transect for this study.

The model (see Fig. 4.15A) has a subducting plate with a lithospheric thickness of 100 km, of which 7 km is crust. The overriding plate has a lithospheric thickness of 150 km, of which 38 km is crust. The plate has been initially subducted for 100 km at a dip of 30 degree. The model is pushed from the side of the overriding plate with a speed of 1.667 cm/year. This value for the velocity is explained in Section 4.5. The outflow in the model is compensated on the same side as the inflow. The model with a weak zone contains two extra compositions. These compositions are placed in a 10 km thick weak zone with a dip of 135 degree (45 degree dipping to the left) to replace the crust and mantle composition up to the bottom of the crust and lithosphere respectively. They differ in properties in three ways from the crust and mantle compositions: A cohesion of 1e4 Pa, an angle of internal friction of 5 degree and a dislocation constant coefficient  $\nu$  of 0.1. The first two make it easier for the plasticity to lower the viscosity, and the last makes the viscosity standard 10 times lower if it is in the dislocation domain. The thermal conductivity of the air in this model is  $200 \text{ W m}^{-1} \text{ K}^{-1}$ . The smallest grid element has a size height and width of 750 meters.

### 4.6.3 Results

The model without the weak zone (Fig. 4.16) took 11.5 days (33% of time solver) to finish nearly 50 Myr years of simulation with 30110 cells and 270872, 33893, 135436 and 135436 Dof for the velocity, pressure, temperature and each composition respectively after the IRS on 116 processors. The amount of cells at about 50 Myr was 36941. This model did not result in rollback of the subduction zone. Instead it showed necking (see c in Fig. 4.16B) and detachment of the slab (Fig. 4.16C) from the subducting plate. What also could be seen were many small scale instabilities and convection cells at the bottom of the lithosphere (see a in figure Fig. 4.16). These instabilities resulted in dripping of lithospheric material into the mantle and thinning of the lithosphere. In areas of large stress, i.e. the crust and the subducting slab, no clear shear-band could be seen. Only a complex viscosity pattern was visible, as can be seen in at locations pointed out by b in Fig. 4.16. These patterns look similar to the complex patterns shown in Fig. 4.2 at C

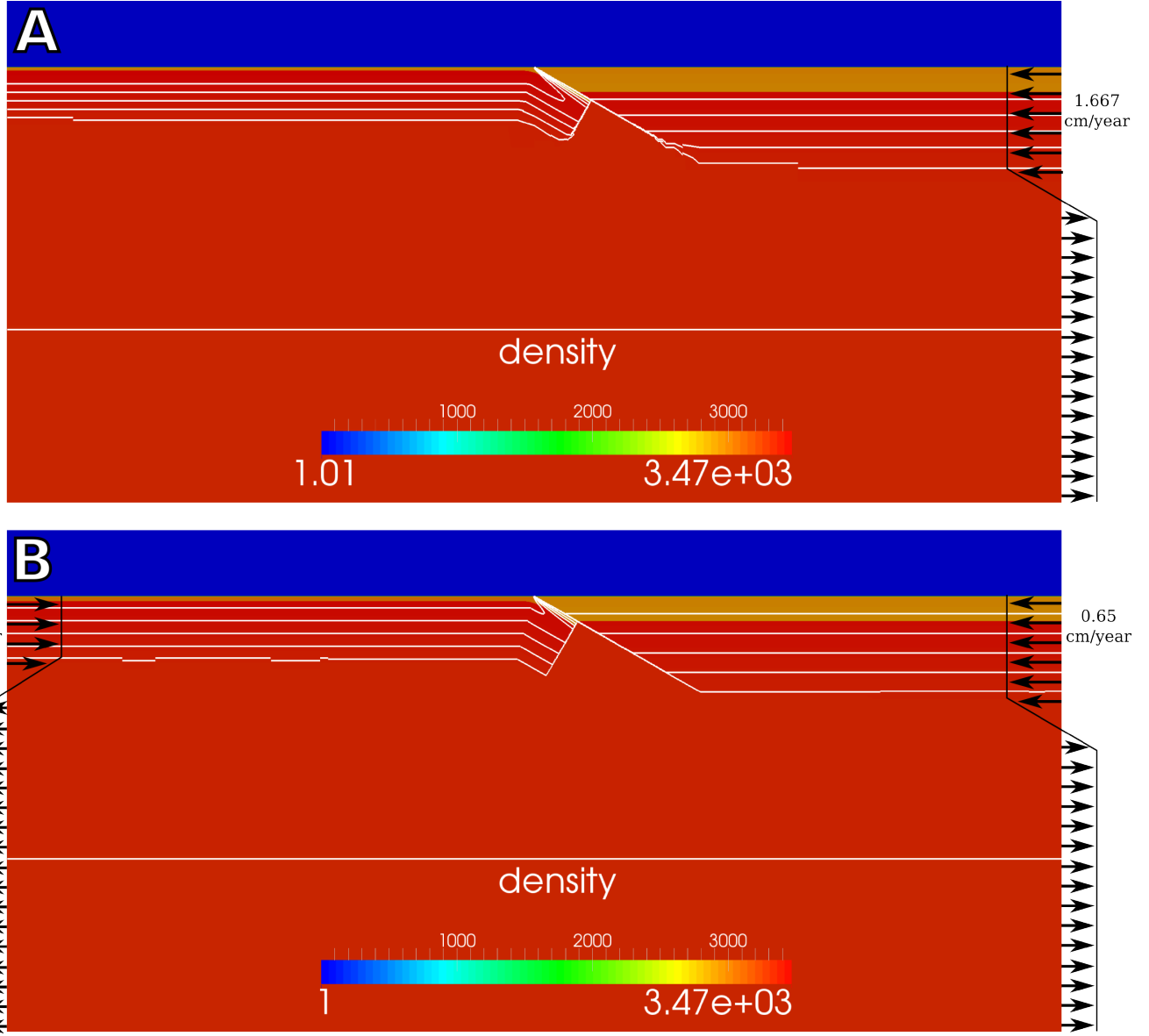


Figure 4.15: The model setup, which shows the density field and temperature isocontours in white before the first timestep. A show the setup described in Section 4.6.2, and B show the adapted setup as described in Section 4.6.3. The black arrows indicate the direction and relative magnitude (not to scale) of the velocity at the boundaries.

and D.

The model with a compositional lithospheric weak zone took 12.5 (83% of time solver) days to finish 10 million years of simulation with 134882 cells and 1111640 Dof for the velocity, 139012 DoF for the pressure and 555820 Dof for the temperature and for each composition after the IRS on 208 processors. The amount of cells at 10 Ma was 108512. The model is shown up to 20 Myr of simulation time in Fig. 4.17. It is currently not possible to go beyond 20 Myr, because the solver was not able to find a solution with a low enough relative residual. The residuals became even larger than the initial residual after 20 Myr. Possible causes for this behaviour are discussed in Section 5.3. The results generated after 10 Myr are for similar reasons considered to be increasingly unreliable. The setup of the model with the weak zone, as shown in Fig. 4.15B, is also a little bit different compared to the model without a weak zone. This is partly due to general improvements to the model and partly to letting the model better represent the case study, but it are mainly changes related to enabling the model to solve for a weak zone as described above. The changes made to the model shown in Fig. 4.17 were, firstly, a higher and stable grid resolution in some areas, secondly, the use of the CRR adaptations with a maximum nonlinear iterations of 150, thirdly, the speed with which

the plates were forced was set to a speed of 1.3 cm/year and was equally divided over both sides, fourthly, the penetration length of the slab was reduced to 76 km and fifthly, the reference density of the crust of the slab was increased to  $3000 \text{ kgm}^{-3}$ .

The solver was not able to solve the model problem for enough simulation time to be able to see whether slab-detachment or rollback would occur. Nevertheless, some interesting features could be observed. Initially, at 50.000 yr simulation time (Fig. 4.17B) the subducting plate contains two zones of shear-bands. A large zone at a, and a smaller zone at b in Fig. 4.17B. Although after 2.5 Myr there still was a zone of lower viscosity at that location pointed out by c in Fig. 4.17C, the shear-band zone had moved much closer to the subduction zone pointed out by d in Fig. 4.17C. At 5 Myr the zone of lower viscosity pointed out by i in Fig. 4.17D had shifted towards the subduction zone and decreased in size and disappears in the following timesteps. The zone of shear-band started to affect the down going slab at about 5 Myr, pointed out by j in Fig. 4.17D. This leads to the smoothing of the hard bend which was still visible at 2.5 Myr at location e in Fig. 4.17C. At 10 Myr, the shear-band had split up in a top section and a lower section pointed out by m in Fig. 4.17E.

The weak zone in the overriding plate in this model was clearly visible, and very active up to 10 Myr. At 10 Myr the weak zone got partially blocked, just below the crust. This happened at the same time as when the part of the overriding plate directly at the subduction zone, pointed out by f in Fig. 4.17, started to subside and increased in viscosity, while at this location it has had a low viscosity and risen for more than 5 Myr. This might indicate that the system was slowly transforming from a compressional system to a system which was in extension. What is furthermore interesting at the weak zone, is that the material of the subduction side of the weak zone which was pushed on the other side of the weak zone caused bending of the edge at location l in Fig. 4.17D and created a zone of clear shear-bands, which had grown (Fig. 4.17E). The mantle part of the overriding plate lithosphere showed an increasing bending of this layer, but at 10 Myr the bend seems slightly less sharp (see Fig. 4.17, right next to the subduction zone at locations g and k in and the same locations at further timesteps). This trend continued at 15 Myr and 20 Myr. This unbending can also be seen as an indicator that the system was transitioning into an extensional system.

The stress state over time can be directly studied with the help of the normal deviatoric stress plugin. This plugin showed both in the x and y direction, that while large parts of the overriding plate were still in compression at 10 Myr, much of the overriding directly next to the subduction zone started to go into an extensional state, which kept growing towards the weak zone at 15 Myr and 20 Myr respectively. The extend of this extensional zone at 20 Myr was about halfway to the subduction zone. It must again be noted that the solutions after 10 Myr are considered to be not completely reliable.

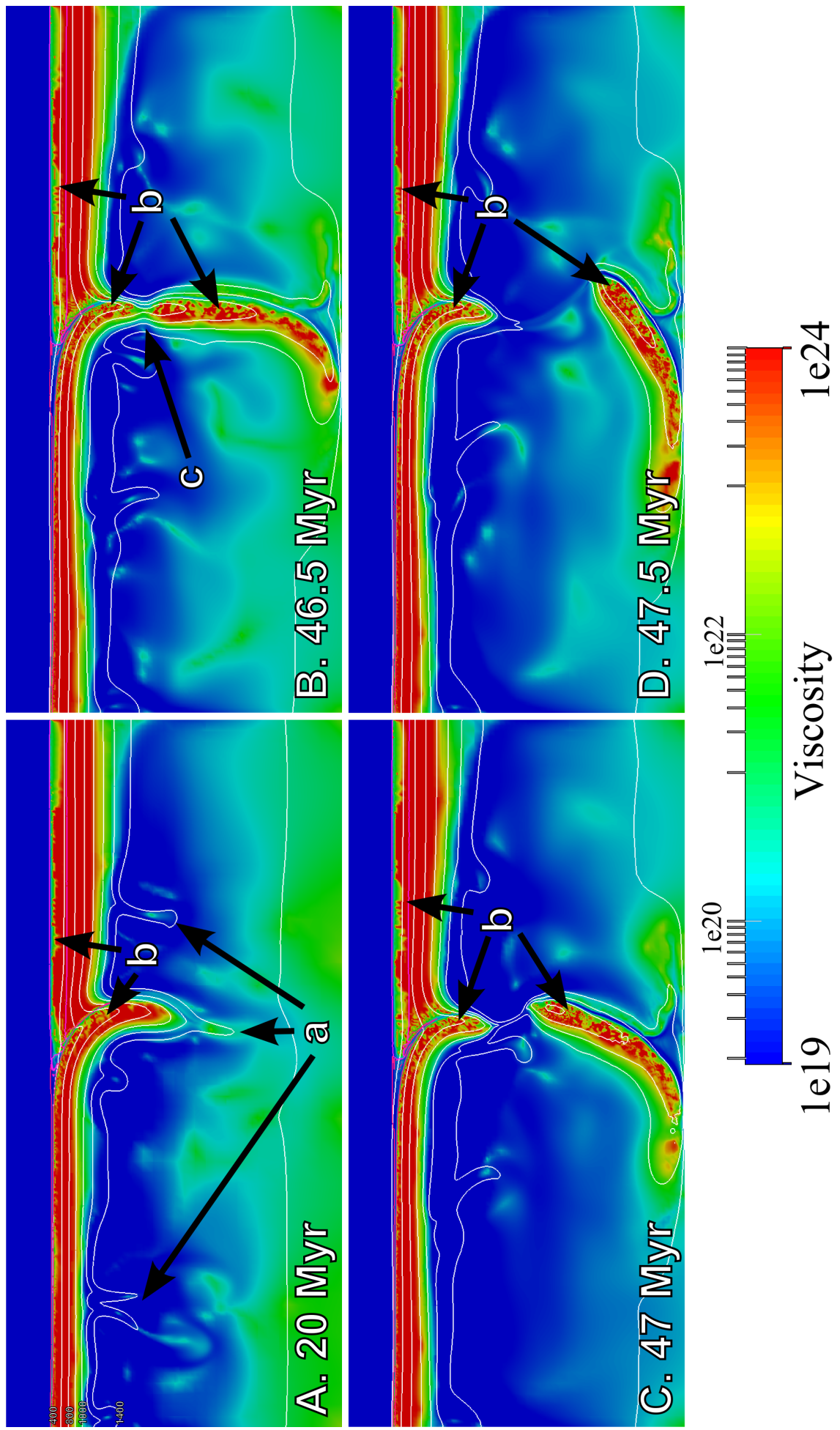


Figure 4.16: Results for the Western Mediterranean subduction modelling case study without the weak zones. The mantle flows from left to right. The white lines are isotherms, and the purple line is the 0.5 isocontour for the crust compositions. A shows small scale instabilities at the bottom of the lithosphere, B shows the complex viscosity patterns in different parts of the model and C shows the necking of the subducting lithosphere.

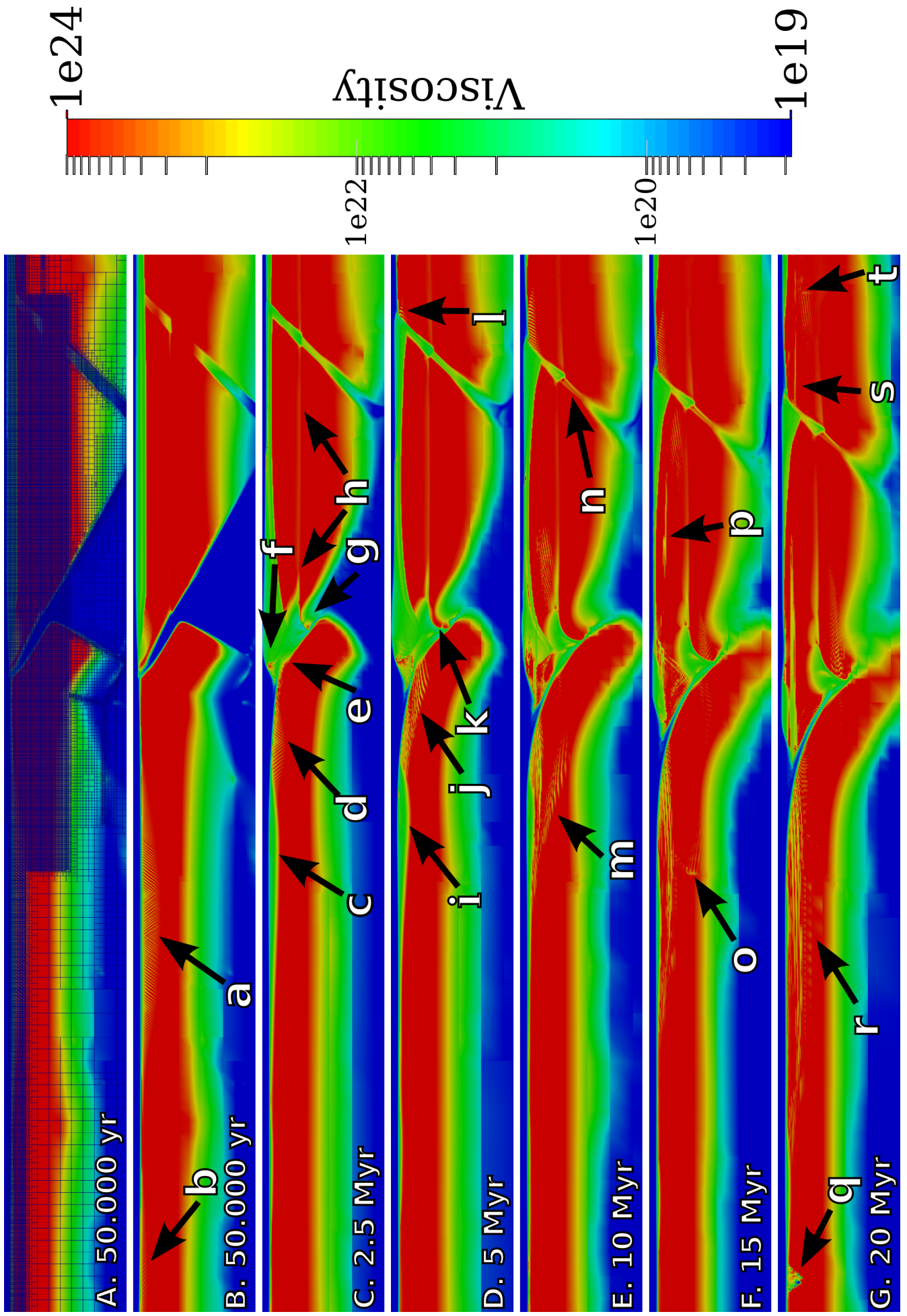


Figure 4.17: A zoom on the subduction zone showing the viscosity field at different times in the simulation. Figure A is overlain with the grid, where the grid is very fine in the dark blue area.

# Chapter 5

## Discussion

### 5.1 General discussion

A 2D modelling study can not account for all the complicated processes in the real earth. Furthermore, 2D model can only be used to study areas where it can be justified that there are no significant 3D effects to be expected. For the chosen area in the Western Mediterranean region, our case study area, this is expected to be only true for the effects which were investigated, i.e. the role of a weak zone and rollback versus slab-detachment. It must also be noted that the zone of interest, the subduction zone, might not be far enough from the model boundaries to be outside its direct influence. Therefore, it should be tested whether increasing the horizontal extend of the model, or implementing and using open boundaries, influences the behaviour and results of the model.

### 5.2 Features and evolution of subduction zone models

With the presented plugins and adaptation of ASPECT, it was shown to be possible to create realistic models of the subduction zones. For the evolution of the subduction zone in these models, it is not required to prescribe a weak zone. The subduction zone also establishes itself at the desired location. This might be due to several factors. One factor is that there is crust material at that location, which is slightly weaker. An other factor comes from the fact that the McKenzie temperature profile in the slab, as explained in Section 3.3.2, assumes that the slab goes directly into the mantle. This leads to a high initial temperature at the top of the subducting slab, which is diffused within a few timesteps. This initial high temperature causes the viscosity to drop, creating an initial weak zone.

All the models showed that the viscosity directly below the lithosphere, especially near the subduction zone, was very low (see for an example Fig. 4.16). Although the viscosity directly below the lithosphere at the left and right edges of the model reached in some models viscosities up to  $10^{21}$ , the viscosities directly below the lithosphere usually were at the minimum limit of  $10^{19}$ . This means that in the model, the viscosity of the upper mantle was the same as the viscosity of the sticky air layer. This is not considered to be a problem for these models, since the sticky air layer is only there to enable topography building. Since the models showed clear topography building, it does not matter that they have the same viscosity.

The thermal properties of the sticky air layer are a problem in a thermo-mechanical model. Real air has a very low thermal conductivity and therefore acts as an isolator. The surface is in reality not isolated by the air, because the air acts on a much shorter timescale due to its very low viscosity. This, and other short time processes in the atmosphere help to keep the surface temperature relatively stable. Because the viscosity of the air in this model is limited to very high values, these stabilisation processes are hardly present. It would be ideal if the boundary condition could be forced directly on the surface, but this is not possible because of the sticky air layer. To let some heat escape from the surface, it is therefore necessary to raise the thermal conductivity. If the thermal conductivity would be raised to infinity, it would directly impose the

top temperature boundary condition to the surface. This effect is a desired effect, as it would simulate the processes keeping the surface temperature stable. The downside of setting a very high thermal conductivity, is that it leads to a very high heat flux, which makes it harder for the solver to reach a solution. In the models, 10 and  $200 \text{ W m}^{-1} \text{ K}^{-1}$  have been chosen as a good compromise. The only major downside was that it lead to temperature anomalies in the air near the subduction zone up to 400 K as at C in Fig. 4.3.

The crust layer in the subduction zone showed in all the models partial detachment and accumulation at the bottom of the lithosphere of the overriding plate as shown at location B in Fig. 4.3. The way this happened over time differed per model. In some models the crust was subducted and only a bit was scraped off, while in other models, crustal material first refused to subduct and accumulated at the bottom of the overriding lithosphere, but when further accumulation was not longer possible, the crust subducted anyway. These kind of crustal detachment effects were expected due to the low density of the crust, making them very buoyant. They have also been observed in many other numerical studies in 2D and 3D, e.g. Currie et al. (2007); Hasenclever et al. (2011).

Another interesting feature in the evolution of the model were the Rayleigh-Taylor type of instabilities at the bottom of the lithosphere pointed out by A in Fig. 4.16. These are instabilities where a lighter fluid is overlain by a heavier fluid, as can be seen in case 1a of van Keeken et al. (1997). In our case, they were purely caused by the temperature. This is because the instabilities were of exactly the same composition as the surrounding material. The low temperature of the lithosphere not only caused the mantle part of the lithosphere to be strong, but also denser than the rest of the upper mantle. In the transition of lithosphere to the asthenosphere, which is a transition from cool to warm material, the material becomes both weaker and less dense. In cases where the bottom of the lithosphere became unstable and dripped off, the density difference, which had become less, became a stronger force then the strength of the material, which is weakened.

### 5.3 AMR and plasticity

AMR is a very good method for saving a lot of computational time by making use of very large cells in areas where not a lot of resolution is required. However, this method also has many problems and pitfalls. The main problem encountered with the AMR in this study had to do, at least partly, with the combination of AMR and plasticity. Firstly, the shear-bands created by the plastic deformation part of the rheology were not capable of running across large difference in the grid fineness as can be seen in Fig. 5.1 and at o and t in Fig. 4.17F. It is also suspected that the chaotic pattern at locations C and D in Fig. 4.2 and at locations B in Fig. 4.16 were the result of a resolution which was changing a lot and/or had a too low resolution in general at that location.

These problems with the sudden change in grid are suspected to lay at the root of the increased relative residual causing the model not to be able to find a good solution. This not only makes sense in theory, the lack of freedom for the lithosphere to internally deform with the help of shear-bands makes the system harder to solve, but is also seen in practice when large shear-band regions disappear at these regions. When the shear-bands start to disappear at the edges of the fine grid at o and t in Fig. 4.17 the relative residuals and the computational time of the timestep start to rise. Indications that the system is not behaving very well can also be seen at various other locations in Fig. 4.17. A very clear example is located at q in Fig. 4.17. This is where the system has tried to compensate for the lack of plastic deformation possibilities. Also note that the feature at q did not penetrate deeper than the very fine resolution area. Also the fact that the shear-band areas, which have always had very clear shear-bands, became very vague and elongated at 15 and 20 Myr in Fig. 4.17. Lastly, at 15 Myr a line at a seemingly random elevation in the crust appeared at location p in Fig. 4.17. At 20 Myr, this line has grown toward the subduction zone. At the other side of the weak zone at location s, which is at the same elevation, a similar line had emerged. Because these lines occurred just above the transition of a high resolution grid to a lower resolution grid, these lines are suspected to also be a symptom of the problem with the AMR and plasticity as described above.

A simple solution seems to be increasing the resolution of the lithosphere to a constant high resolution,

but this may lead to very large systems, which will take a unrealistic amount of time to solve. Although this problem can partially be circumvented by being very careful about where to refine exactly, the general solving speed of the timesteps should also be increased beyond what has been achieved in the tolerance and timing study.

## 5.4 Tracers

The tracer study in Section 4.3 showed that the 0.5 isocontour for the crust composition followed the tracers very well, as can be seen in Fig. 4.4. The tracers usually remained within a quarter of the element size from the 0.5 isocontour. The tracers also showed some problems, which could not all be resolved. One of those problems was the clustering of tracers, of which an example was shown in Fig. 4.4. It shows on the left side two tracers, then in the centre many tracers tightly packed and on the right side of the figure it shows tracers loosely packed. This clustering is strange since all the tracers started at exactly the same distance from each other. It has been suggested by the creators of ASPECT that this might have to do with the advection scheme which might try to save space or calculation time. They have however noted that the tracer part of ASPECT was on the list of items to be completely rewritten. Because the tracer study (Section 4.3) indicated that there was not much accuracy to be gained by the use of tracers next to compositions, and it required significant more time to calculate, the tracer plugin and adaptations have not been used in studies after the tracer study.

## 5.5 Tolerances and speeding up the model

The tolerance study showed that it is possible to speed up the model significantly by adjusting the Stokes tolerance, the nonlinear tolerance and the maximum amount of nonlinear iterations. It must be noted that these results only hold for the specific setup used in this study, and that the exact value are strongly dependent on the model setup. Keeping this in mind, it can be concluded that for this kind of subduction systems the default Stokes tolerance of 1e-7 is too strict. For the tested system it was possible to use a value of 1e-5 without significant consequences for the results. It might be possible to set this value even lower, depending on the setup. Values for the Stokes tolerance of 1e-5 or 1e-6 should be sufficient in most cases. The setting of the value of the nonlinear tolerance also requires special attention, if the CRR adaptions are not used. A too high value for the nonlinear tolerance will cut off the nonlinear iterations before the solution has converged, and a too low value for the nonlinear tolerance will cause continued iterating until the maximum amount of nonlinear iterations is reached. A problem is that the ideal value for the nonlinear tolerance may be completely different at different times in the simulation. Of the methods available for this study, the CRR method is strongly advised. If this method, or a better method is not available, a value of 1e-2 for the nonlinear tolerance can be considered as a good starting point. A good value for the maximum amount of nonlinear iterations is a value of about 100 in most studies. The models usually require 30 to 60 nonlinear iterations before convergence is reached.

The choice of the criterion for cutting off the nonlinear iterations remains a difficult issue. The CRR adaptions provides a better solution than the build in relative residual cut off, but better methods are possible. An example of a better method is described in Thieulot (subm), which is based on direct correlation of one or more fields with the previous version of that field. This is a much more direct way of measuring if a solution has converged or not. This method may save a lot of nonlinear iterations compared to the default ASPECT method and the CRR method.

Not allowing for time for the model to relax has proved in this subduction setting to be beneficial to the value of the Stokes residual. The reason why the residual is a order of magnitude lower when flow is allowed is not completely clear, but it may have to do with the fact that the vertical velocity is always set to zero at the side boundaries in the models. This has as consequence that if there also is no flow in the horizontal direction at the sides, no flow is allowed at all at the boundaries. This may make the whole system much

more rigid and harder to solve. It is currently not possible set from the input file the velocity boundary condition in the horizontal direction and free slip in the vertical direction at the same boundary.

Another possibility for speeding up the model, suggested by the creators of ASPECT, is by setting the Stokes tolerance for the first few nonlinear iterations to a very low value and then increase it slowly to the required level. This has to do with the fact that the first few nonlinear iterations usually take much time because they have to come close to a new good solution.

The overshoots during the Picard iterations are not well understood, but the higher relative residual indicates a bad solution during the overshoot. Fortunately, these overshoots do not seem to hinder the convergence of the nonlinear iterations as a whole. The only danger lies in an overshoot occurring during the last solve of the timestep, which can not be noticed currently in the way the solver is set up.

The time it currently takes to run the models is near the edge of realistic run times. This is a serious limitation converting these kind of models to 3D. They would then have to be simplified substantially, or ASPECT has to be made significantly faster.

## 5.6 Outlook

Since the release of the version which is used for this thesis (the version of 9 December 2013, revision 2111), a lot of new feature have been implemented. Furthermore, some old features still have to be investigated or additional features should be created to be able to make more realistic models. Examples are listed below.

**Strain weakening** Strain weakening is the accumulation of the strain which is then used to lower the viscosity at places where much strain has accumulated. This simulates the process of material breaking up. This process is currently not implemented in ASPECT.

**Phase changes** Phase changes are an important process in the upper mantle, and they can significantly influence the dynamics of a subduction system. A few important phase transitions for subduction systems, which increase the density, are the basalt-eclogite transition at about 50km, the olivine-spinel transition at 410 km and the spinel-perovskite transition at 660 km. They are important because they change the density difference between the cold slab and the warm mantle resisting or helping the subduction process. In the new version of ASPECT latent heat and examples to use it to make phase changes have been implemented.

**Dynamic topography** The use of sticky air works quite well to approximate a real free surface. It costs however a lot of computational time due to the viscosity difference. It can also slow down the simulation by the CLF condition, when the velocity of the air becomes high. An other approach to a free surface is to let the upper nodes of the grid deform vertically based on the velocity field. This approach has been implemented in the new version of ASPECT, but still need to be tested for high deformation cases like subduction settings.

**Melting** Melting is an important process in a subduction setting. It helps removing the crust from the subducting slab, heats the lower crust of the overriding plate and creates the volcanic arc in the overriding plate. It can not only influence the dynamics, but it can also be used to compare the model results with chemistry data.

**Surface processes** At the moment it is possible to build up topography due to tectonic processes. However, there are no surface processes to break down high elevation and fill low elevation. Surface processes have shown to be an influence on deep tectonic processes (e.g. Beaumont et al., 1992; Burov and Toussaint, 2007), and have not been implemented in ASPECT.

**Stress/open boundaries** It is known that the boundaries of a model can strongly influence its behaviour (Chertova et al., 2012). This influence can be reduced by creating a lot of space between the zone of interest and the boundaries. This approach requires much computational power. Open boundaries, which are boundaries which have been assigned a stress equal to the lithostatic pressure, have shown to be a good replacement for a large part of this extra space beside the zone of interest. Implementation of a open boundary condition requires the implementation of stress boundaries into ASPECT.

**Better refinement options** Controlling the AMR remains a challenge. There are now options available in ASPECT to directly change the refinement flag without going through the error field. A very promising method in the case of subduction modelling to solve the problem with the AMR is to force a certain refinement level based on temperature. It would then set every cell at that refinement level if the temperature is below a certain value. If a sticky air layer is used, it should then also be possible to limit it at a certain elevation.

**Newton-Raphson iterations** As described in Section 3.1.5.2, ASPECT uses Picard type of iterations for solving coupled nonlinear systems. More robust and efficient iterative methods, such as the Newton-Raphson method (Ismail-Zadeh and Tackley, 2010), could be implemented into ASPECT. However, the implementation of this method is considered to be difficult, and requires a good initial guess (Le Pourhiet, 2013). This is because this method only has local convergence, thus a few Picard iterations are required.

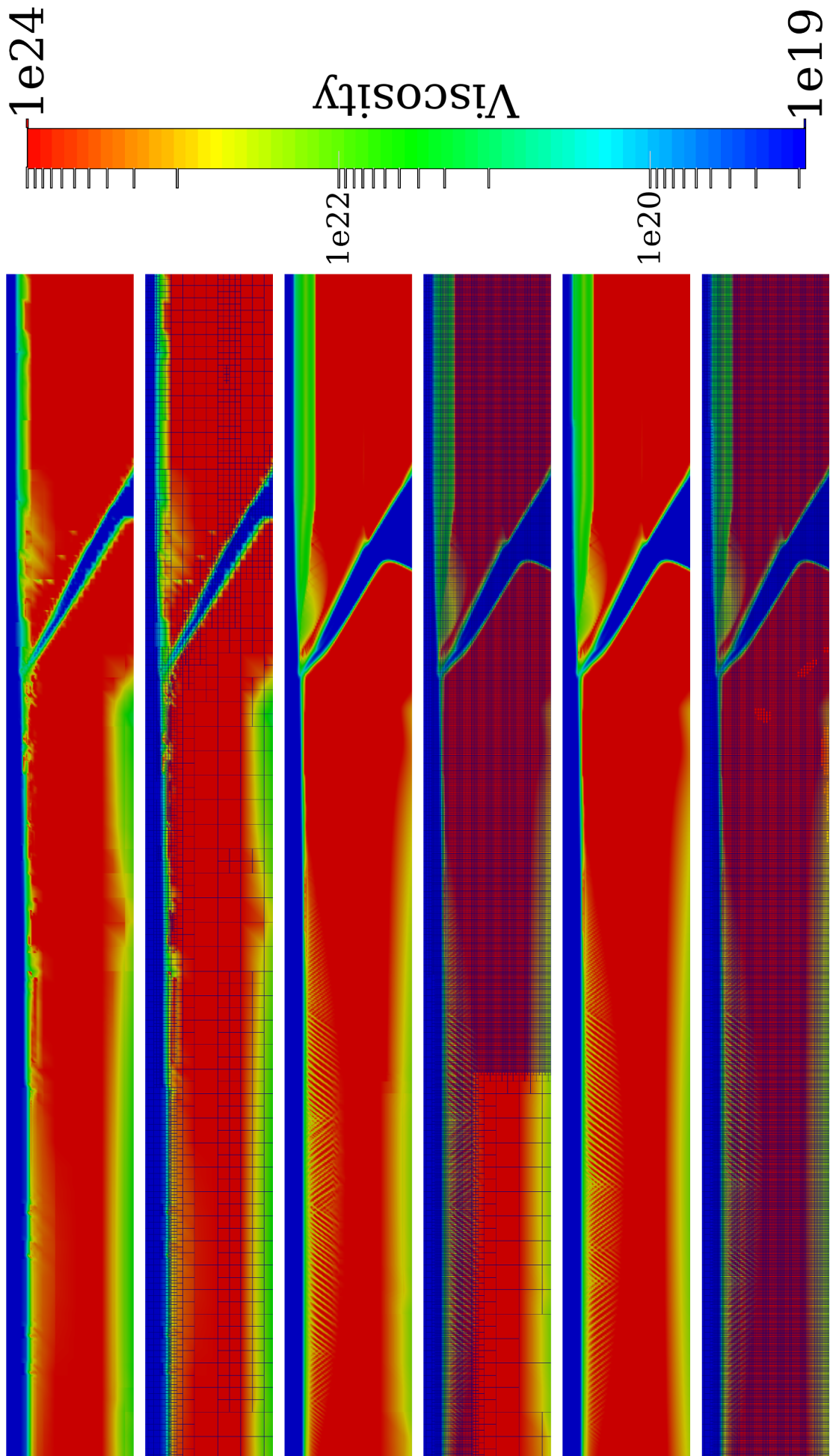


Figure 5.1: The influence of grid fineness on the plastic deformation pattern after a few timesteps. A, C and E show the results for the viscosity field and B, D and F show those results overlaid with the used grid.

# Chapter 6

## Conclusions and recommendations

The mantle convection code ASPECT has shown to be a promising and versatile code, capable of more than it is built for. With the presented plugins and adaptation of ASPECT, we have been able to create the first thermomechanical subduction model, also capable of building topography, with this code designed for mantle convection. This framework of the ASPECT code with the new plugins and adaptations provides a versatile code base not only fit for building diverse subduction models, but also for other type of models which can be built from this framework.

The whole framework of ASPECT and the new plugins and adaptations have been thoroughly tested, both in performance and results with satisfactorily results and several recommendations for further improvements. The recommendations for further improvements regard recommendations for settings in ASPECT and the new plugins and adaptations as well as recommendations for additional plugins and adaptations to ASPECT. The recommendations are:

1. When plasticity is used in a model, all the places where it can occur should have the same, high resolution grid. A good solution to achieve this may be partly present in the newer version of ASPECT.
2. The default ASPECT stokes tolerance of 1e-7 is too strict in all shown cases, and a tolerance of 1e-5 to 1e-6 is recommended as a good starting point for own investigation.
3. The default stopping criterion for the nonlinear iterations, which uses a tolerance for the relative residual, is not sufficient. Although the new CRR method is an improvement, the implementations of other methods based on the correlation of the fields is recommended.
4. The passive tracers currently implemented in ASPECT show behaviours during the advection which can not be fully explained yet, and the use of these tracers in ASPECT is therefore currently not recommended.
5. The tested models showed that directly pushing the plates from the sides, instead of letting them relax first, results in a faster convergence and residuals which are an order of magnitude lower. It is recommended to investigate this kind of behaviour per model.
6. We recommend the implementation of the following new features to the subduction model, or ASPECT in general to be able to make more realistic models: strain weakening, phase changes, dynamic topography, melting, open/stress boundaries and surface processes.

The combination of the ASPECT code with a set of plugins and adaptations has been tested for a general subduction case, and shows processes which are similar to what is thought to happen in the real earth. The specific case study for the Mediterranean region showed slab detachment instead of rollback, which is suspected to have a physical background. We were not able to validate the hypothesis for whether a lithospheric weak zone could allow the system to go into a rollback mode, due to numerical problems during the simulation. Nevertheless, some indications were obtained that it may play a significant role.

# Bibliography

- Advokaat, E. L., van Hinsbergen, D. J., Maffione, M., Langereis, C. G., Vissers, R. L., Cherchi, A., Schroeder, R., Madani, H., and Columbu, S. (2014). Eocene rotation of Sardinia, and the paleogeography of the western Mediterranean region. *Earth Planet. Sci. Lett.*, 401:183–195.
- Anderson, J. (1995). *Computational Fluid Dynamics*. McGraw-Hill.
- Baitsch-Ghirardello, B., Gerya, T. V., and Burg, J. P. (2014). Geodynamic regimes of intra-oceanic subduction: Implications for arc extension vs. shortening processes . *Gondwana Research*, 25(2):546 – 560.
- Bangerth, W., Hartmann, R., and Kanschat, G. (2007). Deal.II - a general purpose object oriented finite element library. *ACM Trans. Math. Softw.*, 33(4):1–24:27.
- Bangerth, W., Heister, T., et al. (2014). *ASPECT: Advanced Solver for Problems in Earth's Convection*. Computational Infrastructure in Geodynamics.
- Baumann, C., Gerya, T., and Connolly, J. A. D. (2008). Numerical modeling of spontaneous slab break-off dynamics during continental collision. In Spalla, M. I., Marotta, A. M., and Gosso, G., editors, *Advances in Interpretation of Geological Processes*, volume 332, pages 99–114. Geological Society, London.
- Beaumont, C., Fullsack, P., and Hamilton, J. (1992). Erosional control of active compressional orogens. In McClay, K. R., editor, *Erosional control of active compressional orogens*, volume 1, pages 1–18. Springer Netherlands.
- Behounkova, M. and Čížková, H. (2008). Long-wavelength character of subducted slabs in the lower mantle. *Earth Planet. Sci. Lett.*, 275:43–45.
- Boussinesq, J. (1897). *Théorie de l'écoulement tourbillonnant et tumultueux des liquides dans les lits rectilignes à grande section*, volume 1. Gauthier-Villars.
- Braun, J., Thieulot, C., Fullsack, P., DeKool, M., and Huismans, R. (2008). DOUAR: a new three-dimensional creeping flow model for the solution of geological problems. *Phys. Earth. Planet. Inter.*, 171:76–91.
- Burkett, E. and Billen, M. (2010). Three-dimensionality of slab detachment due to ridge-trench collision: Laterally simultaneous boudinage versus tear propagation. *Geochem. Geophys. Geosyst.*, 11(11).
- Burov, E., Francois, T., Agard, P., Le Pourhiet, L., Meyer, B., Tirel, C., Lebedev, S., Yamato, P., and Brun, J.-P. (2014). Rheological and geodynamic controls on the mechanisms of subduction and HP/UHP exhumation of crustal rocks during continental collision: Insights from numerical models. *Tectonophysics*.
- Burov, E. and Toussaint, G. (2007). Surface processes and tectonics: Forcing of continental subduction and deep processes. *Global and Planetary Change*, 58:141–164.
- Burstedde, C., Wilcox, L. C., and Ghattas, O. (2011). *p4est*: Scalable algorithms for parallel adaptive mesh refinement on forests of octrees. *SIAM Journal on Scientific Computing*, 33(3):1103–1133.
- Cagnioncle, A., Parmentier, E. M., and Elkins-Tanton, L. T. (2007). Effect of solid flow above a subducting slab on water distribution and melting at convergent plate boundaries. *J. Geophys. Res.*, 112:B09402.

- Cai, Y., Wang, Y., Cawood, P. A., Fan, W., Liu, H., Xing, X., and Zhang, Y. (2014). Neoproterozoic subduction along the Ailaoshan zone, South China: Geochronological and geochemical evidence from amphibolite. *Precambrian Research*, 245(0):13 – 28.
- Capitanio, F., Morra, G., and Goes, S. (2007). Dynamic models of downgoing plate-buoyancy driven subduction: subduction motions and energy dissipation. *Earth Planet. Sci. Lett.*, 262:284–297.
- Carminati, E., Doglioni, C., Gelabert, B., Panza, G., Raykova, R., Roca, E., Sabat, F., and Scrocca, D. (2012). 12 - Evolution of the Western Mediterranean. In Roberts, D. and Bally, A., editors, *Regional Geology and Tectonics: Phanerozoic Passive Margins, Cratonic Basins and Global Tectonic Maps*, pages 436 – 470. Elsevier, Boston.
- Chertova, M., Geenen, T., van den Berg, A., and Spakman, W. (2012). Using open sidewalls for modelling self-consistent lithosphere subduction dynamics . *Solid Earth*, 3:313–326.
- Chertova, M., Spakman, W., Geenen, T., van den Berg, A., and van Hinsbergen, D. (2014). Underpinning tectonic reconstructions of the western Mediterranean region through dynamic slab evolution from 3D numerical modeling. *J. Geophys. Res.*
- Crameri, F. and Kaus, B. (2010). Parameters that control lithospheric-scale thermal localization on terrestrial planets. *Geophys. Res. Lett.*, 37(L09308).
- Crameri, F., Schmeling, H., Golabek, G., Duretz, T., Orendt, R., Buiter, S., May, D., Kaus, B., Gerya, T., and Tackley, P. (2012). A comparison of numerical surface topography calculations in geodynamic modelling: an evaluation of the 'sticky air' method. *Geophys. J. Int.*, 189:38–54.
- Currie, C., Beaumont, C., and Huismans, R. (2007). The fate of subducted sediments: a case for backarc intrusion and underplating. *Geology*, 35(12):1111–1114.
- Donea, J. and Huerta, A. (2003). *Finite Element Methods for Flow Problems*. John Wiley & Sons.
- Duretz, T., Gerya, T., Kaus, B., and Andersen, T. (2012). Thermomechanical modeling of slab eduction. *J. Geophys. Res.*, 117(B08411).
- Duretz, T., Gerya, T., and May, D. (2011). Numerical modelling of spontaneous slab break-off and subsequent topography response. *Tectonophysics*, 502:244–256.
- Faccenna, C., Becker, T. W., Lucente, F. P., Jolivet, L., and Rossetti, F. (2001a). History of subduction and back-arc extension in the Central Mediterranean. *Geophys. J. Int.*, 145:809–820.
- Faccenna, C., Funiciello, F., Giardini, D., and Lucente, P. (2001b). Episodic back-arc extension during restricted mantle convection in the Central Mediterranean. *Earth Planet. Sci. Lett.*, 187:105–116.
- Faccenna, C., Piromallo, C., Crespo-Blanc, A., Jolivet, L., and Rossetti, F. (2004). Lateral slab deformation and the origin of the western Mediterranean arcs. *Tectonics*, 23(TC1012).
- Frisch, W. (1979). Tectonic progradation and plate tectonic evolution of the Alps. *Tectonophysics*, 60:121–139.
- Garel, F., Goes, S., Davies, D. R., Davies, J. H., Kramer, S. C., and Wilson, C. R. (2014). Interaction of subducted slabs with the mantle transition-zone: A regime diagram from 2-D thermo-mechanical models with a mobile trench and an overriding plate. *Geochem. Geophys. Geosyst.*, 15:1739–1765.
- Gerya, T. (2010). *Numerical Geodynamic Modelling*. Cambridge University Press.
- Gerya, T. (2011). Future directions in subduction modeling. *Journal of Geodynamics*, 52:344–378.
- Gerya, T. and Yuen, D. (2003a). Characteristics-based marker-in-cell method with conservative finite-differences schemes for modeling geological flows with strongly variable transport properties. *Phys. Earth. Planet. Inter.*, 140:293–318.
- Gerya, T. and Yuen, D. (2003b). Rayleigh-Taylor instabilities form hydration and melting propel 'cold plumes' at subduction zones. *Earth Planet. Sci. Lett.*, 212:293–318.

- Gerya, T. and Yuen, D. (2007). Robust characteristics method for modelling multiphase visco-elasto-plastic thermo-mechanical problems. *Phys. Earth. Planet. Inter.*, 163:83–105.
- Glerum, A. C. (2014). Personal communications.
- Govers, R. and Wortel, M. (1995). Extension of stable continental lithosphere and the initiation of lithospheric scale faults. *Tectonics*, 14(4):1041–1055.
- Guermond, J.-L., Pasquetti, R., and Popov, B. (2011). Entropy viscosity method for nonlinear conservation laws. *Journal of Computational Physics*, 230(11):4248 – 4267. Special issue High Order Methods for CFD Problems.
- Gurnis, M., Hall, C., and Lavier, L. (2004). Evolving force balance during incipient subduction. *Geochem. Geophys. Geosyst.*, 5(7).
- Handy, M. R., Schmid, S. M., Bousquet, R., Kissling, E., and Bernoulli, D. (2010). Reconciling plate-tectonic reconstructions of Alpine Tethys with the geological-geophysical record of spreading and subduction in the Alps. *Earth-Science Reviews*, 102:121–158.
- Hansen, V. (2007). Subduction origin on early Earth: a hypothesis. 35:1059–1062.
- Hasenclever, J., Morgan, J. P., Hort, M., and Rüpke, L. H. (2011). 2D and 3D numerical models on compositionally buoyant diapirs in the mantle wedge. *Earth Planet. Sci. Lett.*, 311(1-2):53–68.
- Herbert, L. B., Antoshechkina, P., Asimow, P., and Gurnis, M. (2009). Emergence of a low-viscosity channel in subduction zones through the coupling of mantle flow and thermodynamics. *Earth Planet. Sci. Lett.*, 278:243–256.
- Heroux, M. A., Bartlett, R. A., Howle, V. E., Hoekstra, R. J., Hu, J. J., Kolda, T. G., Lehoucq, R. B., Long, K. R., Pawlowski, R. P., Phipps, E. T., Salinger, A. G., Thornquist, H. K., Tuminaro, R. S., Willenbring, J. M., Williams, A., and Stanley, K. S. (2005). An overview of the Trilinos project. *ACM Trans. Math. Softw.*, 31(3):397–423.
- Hetényi, G., Godard, V., Cattin, R., and Connolly, J. (2011). Incorporating metamorphism in geodynamic models: the mass conservation problem. *Geophys. J. Int.*, 186:6–10.
- Hillebrand, B., Thieulot, C., Geenen, T., van den Berg, A., and Spakman, W. (subm.). Using the level set method in geodynamical modeling of multi-material flows and Earth's free surface. *Solid Earth*.
- Ismail-Zadeh, A. and Tackley, P. (2010). *Computational Methods for Geodynamics*. Cambridge University Press.
- Jadamec, M. A., Billen, M. I., and Roeske, S. M. (2013). Three-dimensional numerical models of flat slab subduction and the Denali fault driving deformation in south-central Alaska. *Earth and Planetary Science Letters*, 376(0):29 – 42.
- Kameyama, M., Yuen, D., and Karato, S.-I. (1999). Thermal-mechanical effects of low-temperature plasticity (the Peierls mechanism) on the deformation of a viscoelastic shear zone. *Earth Planet. Sci. Lett.*, 168:159–172.
- Karato, S.-I. (2008). *Deformation of Earth Materials*. Cambridge University Press.
- Kronbichler, M., Heister, T., and Bangerth, W. (2012). High accuracy mantle convection simulation through modern numerical methods . *Geophys. J. Int.*, 191:12–29.
- Le Pourhiet, L. (2013). Plasticity and strain localisation in the crust and lithosphere models: Numerical aspects. In *LUCKY #13: XIII International Workshop on Modelling of Mantle and Lithosphere Dynamics*. <http://www.earthdynamics.org/lucky13/publications/talks/LePourhiet.pdf>.
- Lenardic, A. and Kaula, W. (1993). A numerical treatment of geodynamic viscous flow problems involving the advection of material interfaces. *J. Geophys. Res.*, 98(B5):8243–8260.

- Loiselet, C., Braun, J., Husson, L., Le Carlier de Veslud, C., Thieulot, C., Yamato, P., and Grujic, D. (2010). Subducting slabs: Jellyfishes in the Earth's mantle. *Geochem. Geophys. Geosyst.*, 11(8):doi:10.1029/2010GC003172.
- McKenzie, D. P. (1970). Temperature and potential temperature beneath island arcs. *Tectonophysics*, 10:357–366.
- McNamara, A. and Zhong, S. (2004). Thermochemical structures within a spherical mantle: Superplumes or Piles? *J. Geophys. Res.*, 109(B07402).
- Meister, A. (1999). *Numerik linearer Gleichungssysteme*. Vieweg+Teubner, fourth edition.
- Moresi, L., Dufour, F., and Muhlhaus, H. (2003). A Lagrangian integration point finite element method for large deformation modeling of visco-elastic geomaterials. *J. Comp. Phys.*, 184:476–497.
- Moresi, L., Quenette, S., Lemiale, V., Mériaux, C., Appelbe, B., and Mühlhaus, H.-B. (2007). Computational approaches to studying non-linear dynamics of the crust and mantle. *Phys. Earth. Planet. Inter.*, 163:69–82.
- Nikolaeva, K., Gerya, T., and Marques, F. (2011). Numerical analysis of subduction initiation risk along the Atlantic American margins. *Geology*, 39:463–466.
- OzBench, M., Regenauer-Lieb, K., Stegman, D., Morra, G., Farrington, R., Hale, A., May, D., Freeman, J., Bourgoin, L., Mühlhaus, H.-B., and Moresi, L. (2008). A model comparison study of large-scale mantle-lithosphere dynamics driven by subduction. *Phys. Earth. Planet. Inter.*, 171:224–234.
- Quinquis, M. E., Buitter, S. J., and Ellis, S. (2011). The role of boundary conditions in numerical models of subduction zone dynamics. *Tectonophysics*, 497:57–70.
- Schmeling, H., Babeyko, A., Enns, A., Faccenna, C., Funiciello, F., Gerya, T., Golabek, G., Grigull, S., Kaus, B., Morra, G., Schmalholz, S., and van Hunen, J. (2008). A benchmark comparison of spontaneous subduction models - Towards a free surface. *Phys. Earth. Planet. Inter.*, 171:198–223.
- Schubert, G., Turcotte, D. L., and Olson, P. (2001). *Mantle Convection in the Earth and Planets*. Cambridge University Press.
- Solomatov, V. (2004). Initiation of subduction by small-scale convection. *J. Geophys. Res.*, 109(B01412).
- Song, S., Niu, Y., Su, L., Zhang, C., and Zhang, L. (2014). Continental orogenesis from ocean subduction, continent collision/subduction, to orogen collapse, and orogen recycling: The example of the Qorth Qaidam UHPM belt, NW China. *Earth-Science Reviews*, 129(0):59 – 84.
- Spakman, W. and Wortel, M. (2004). A tomographic view on Western Mediterranean Geodynamics. In Cavazza, W., Roure, F., Spakman, W., Stampfli, G. M., and Ziegler, P., editors, *TRANSMED Atlas, The Mediterranean Region from Crust to Mantle*, pages 31–52.
- Strobl, M., Hetzel, R., Fassoulas, C., and Kubik, P. (2014). A long-term rock uplift rate for Eastern Crete and geodynamic implications for the Hellenic subduction zone. *Journal of Geodynamics*, 78(0):21 – 31.
- Tan, E., Choi, E., Thoutireddy, P., Gurnis, M., and Aivazis, M. (2006). GeoFramework: Coupling multiple models of mantle convection within a computational framework. *Geochem. Geophys. Geosyst.*, 7(Q06001).
- Thieulot, C. (2011). FANTOM: two- and three-dimensional numerical modelling of creeping flows for the solution of geological problems. *Phys. Earth. Planet. Inter.*, 188:47–68.
- Thieulot, C. (subm.). ELEFANT: a user-friendly multipurpose geodynamics code. *Solid Earth*.
- van Hinsbergen, D. J. J., Vissers, R. L. M., and Spakman, W. (2014). Origin and Consequences of western Mediterranean subduction, rollback and slab segmentation. *Tectonics*, 33.
- van Hunen, J. and Allen, M. B. (2011). Continental collision and slab break-off: A comparison of 3-D numerical models with observations. *Earth and Planetary Science Letters*, 302(1-2):27 – 37.

- van Keken, P., King, S., Schmeling, H., Christensen, U., Neumeister, D., and Doin, M.-P. (1997). A comparison of methods for the modeling of thermochemical convection. *J. Geophys. Res.*, 102(B10):22,477–22,495.
- van Keken, P. E., Currie, C., King, S. D., Behn, M. D., Cagnioncle, A., He, J., Katz, R. F., Lin, S., Parmentier, E. M., Spiegelman, M., and Wang, K. (2008). A community benchmark for subduction zone modelling. *Phys. Earth. Planet. Inter.*, 171:187–197.
- Vissers, R. L. M., van Hinsbergen, D. J. J., and Meijer, P. T. (2013). Kinematics of Jurassic ultra-slow spreading in the Piemonte Ligurian ocean. *Earth Planet. Sci. Lett.*, 380:138–150.
- Zaleski, S. and Julien, P. (1992). Numerical simulation of Rayleigh-Taylor instability for single and multiple salt diapirs. *Tectonophysics*, 206:55–69.
- Zhong, S., Zuber, M., Moresi, L., and Gurnis, M. (2000). The role of temperature-dependent viscosity and surface plates in spherical shell models of mantle convection. *J. Geophys. Res.*, 105:11,063–11,082.
- Zlotnik, S., Fernandez, M., Diez, P., and Verges, J. (2008). Modelling gravitational instabilities: slab break-off and Rayleigh-Taylor diapirism. *Pure appl. geophys.*, 165:1491–1510.

# Glossary

**compositional field** A method to track material, which defines for every place in the model if it is inside or outside the material.

**DEAL.II** A general purpose finite element library. It communicates for ASPECT with other libraries and handles everything that has to do with meshes, finite elements and discretization.

**direct solver** A solver which can directly compute the exact solution of a linear problem.

**inner iteration** This is a loop where the iterative solver tries to converge to the exact solution of the linear system.

**input file** A structured file in which the parameters a model uses can be easily changed between models.

**iterative solver** A solver which iterates towards the exact solution of a linear problem.

**levelset** A method to track material by defining isocontours and functions.

**library** A collection of code and subprograms designed to be used by other programs.

**linear solver tolerance** The magnitude the residual is allowed to deviate from zero.

**marker** A method to track material by defining 'physical' particles in the model. There are two versions: passive, which just contains environmental data and active which also contains parameters which are used in the calculation.

**nonlinear solver tolerance** The magnitude the relative residual is allowed to deviate from zero.

**outer iteration** This is a loop where the exact solution of the solver (which has finished the inner iterations) is taken as a starting point to calculate a new solution. This is done until the system is converged.

**p4est** A library which is designed to build distributed adaptive meshes.

**plugin** A small self contained piece code, with a specific function which can be easily attached and removed from the main program to add or remove functionality.

**relative residual** This is the current residual divided by the first residual of the unsolved system of the current timestep.

**residual** This is the  $l_2$  norm of  $R$  in  $R = \mathbf{A}x - b$ .

**solver** A code or program designed to solve a system of equations.

**sticky air** A method to create a free surface by putting a low viscosity layer on top of the model.

**tracer** See marker.

**TRILINOS** A parallel linear algebra library, which provides solvers to ASPECT.

# Acronyms

**AMR** Adaptive Mesh Refinement.

**ASPECT** Advanced Solver for Problems in Earth's ConvecTion.

**CFL** Courant-Friedrich-Lewy.

**CR**R Converged Relative residual.

**DoF** Degrees of Freedom.

**FEM** Finite Element Method.

**IRS** Initial Refinement Steps.

**MPI** Message Passing Interface.

**NBTZ** North Balearic Transform zone.

**rhs** right hand side.